LUND UNIVERSITY
Faculty of Science

Fundamental combustion properties of alternative fuels for energy transition

Yijing Mao

Thesis submitted for the degree of Master of Science
Project duration: 8 months

Supervised by Christian Brackmann and Marco Lubrano Lavadera

Department of Physics
Division of Combustion Physics
May 2020

Abstract

Validation and improvement of chemical kinetic modelling require accurate experimental data. The over goal of the present work is to obtain accurate data by using techniques that have been previously implemented in common flames, e.g. of methane, and showed good performance to provide high-value input for model validation of dimethyl ether (DME) combustion. Measurements of laminar burning velocity of premixed DME/air flames at standard pressure, elevated unburned gas mixture temperature 298-338 K, and at equivalence ratios $\Phi = 0.7\text{-}1.6$ were performed by using the heat flux method that can create one-dimensional, non-stretched, adiabatic flames. In addition, the nitric oxide (NO) formation in the post-flame zone at the initial gas mixtures temperature of 338 K and atmospheric pressure was quantitatively studied by employing the calibrated saturated laser-induced fluorescence technique. The temperature dependence of the burning velocity was derived from the experimental results. The acquired data in terms of burning velocity and NO mole fraction were compared with literature data and predictions of six existing mechanisms. Simulation results from a model by Konnov et al. and the POLIMI CRECK mechanism agreed well with experimental data. The data can be considered as highly valuable input for continued model validation and development.

Contents

List of Acronyms and abbreviations

DME	Dimethyl Ether
NO	Nitric Oxide
NO_x	Nitrogen Oxides
LIF	Laser-induced Fluorescence
LSF	Saturated Laser-induced Fluorescence
ASDT	Annular Stepwise Diverging Tube
ADT	Annular Diverging Tube
RET	Rotational Energy Transfer
MFCs	Mass Flow Controllers
PMT	Photomultiplier Tube

1. Introduction

1.1. The requirement for alternative fuels

Nowadays, combustion is one of the main ways of energy production in the world. It is widely used in important fields such as electricity generation, transportation, waste incineration, etc. However, "greenhouse gas" CO_2 and air pollutants are generated during combustion processes, which cause serious environmental problems. One of the air pollutants nitrogen oxides (NO_x) are not only the main substances that form acid rain, but also important substances that form photo-chemical smog in the atmosphere and a significant factor that consumes ozone (O_3) [1]. In addition, NO_x also have negative effect on human health. They can damage the central nervous system of the human body, cause breathing problems, reduce lung function, etc. [2]. Moreover, the available fossil energy sources, such as petroleum, natural gas, and coal are gradually decreasing. All of them are non-renewable resources. Thus, suitable low-emission and renewable alternative fuels are required.

Dimethyl ether (DME; CH_3-O-CH_3) is the simplest ether with low boiling point (-25℃ at 1 atm) [3]. It has similar physical properties compared to liquefied petroleum gas. Since there is no C-C bond in the molecular structure of DME, its combustion shows soot-free characteristics. In addition, Hwang et al. have numerically shown that DME generates lower NO_x emissions than other hydrocarbon fuels [4]. Moreover, due to the fact that the cetane number[1] of some widely used fuels such as liquefied petroleum gas and C_1-C_2 alcohol fuels is lower than 10, these poorly flammable fuels are only suitable for spark ignition engines. However, the cetane number of DME is between 55-60 and it has excellent compressibility [5]. Given these physical-chemical properties, DME is very suitable for applying in compression ignition engines. Therefore, compared with other alternative fuels such as methane, methanol, and ethanol, DME has greater potential to replace traditional fuels in terms of pollutant emissions, energy efficiency, usability, economics, etc.

However, despite that DME has many advantages as an alternative fuel, in order to widely use it in practical applications, it is necessary to study its combustion behavior in detail. To achieve this goal, detailed studies on the flame structure, ignition delay time, laminar burning velocity, and combustion products of the DME + oxidizer mixtures are required.

1.2. State of the art

Over the past two decades, researchers have developed many experimental methods [6-20] and chemical kinetic models [21-30] for the laminar burning velocity (S_L)

[1] An index indicating the ignitibility of diesel, and the ignitibility is proportional to the value.

measurement and prediction of DME at standard ambient temperature and pressure. However, there is a large dispersion among the experimental data and simulation results of chemical kinetic models, especially at fuel-rich conditions.

Among these experimental methods, the spherical flame method is one of the most popular techniques for measuring the laminar burning velocity of DME/air mixtures. Daly et al. [14] were the first authors that employed this technique to study laminar burning velocity with the equivalence ratio within 0.7-1.7 at standard ambient temperature and pressure. With this method, mixtures of fuel and oxidizer are ignited in a closed vessel, and the flame propagation velocity can be derived from the relationship between the flame radius and time or pressure and time. However, experimental data measured by this method are scattered, with about 50-80% disagreement between the group of Huang et al. [13] and Zhao et al. [7]. Another commonly used method for obtaining burning velocity of DME/air mixtures is the stagnation flame method. When the flame reaches stable conditions, the smallest unburned gas velocity can be regarded as the flame propagation speed. Since the flames obtained by these two techniques are stretched, in order to derive the flame speed, flame stretch correction using extrapolation methods is required. In the 1980s, linear flame stretch corrections were reported by Wu et al.[31], Lewis et al. [32], and Matalon et al. [33,34]. However, it is well known that there are inevitable errors in the linear extrapolation method, and van Maaren et al. [35] proved that the linear flame stretch correction may lead to higher results. Then, Chao et al. [36] introduced the non-linear flame stretch correction, and Wang et al. [6] employed this method in their research. The heat flux method, which can directly measure the laminar burning velocity without any flame stretch correction, was given by de Goey et al. in 1993, and Wang et al. [17] have implemented this method to measure the laminar burning velocity of premixed DME/air mixtures blended with methane at various mixture fractions in 2018. This method is based on the use of an external heating system to compensate for the heat loss required to stabilize the flame to achieve a one-dimensional, stretch-free, adiabatic flame. Recently, two relatively new measurement methods: the annual stepwise diverging tube [19,20] and externally heated diverging channel method [18] have also been developed and applied to measure the laminar burning velocity of DME/air mixtures. In both methods, the laminar burning velocity is derived from the mass conservation at the flame front. However, in order to obtain more accurate data, problems due to heat losses, hydrodynamic stretching, and flame stability still need to be resolved in these new techniques.

For the study of combustion emissions, researchers have paid more attention on nitrogen oxides (NO_x). In order to reduce or remove NO_x, several methods have been developed. For example, selective catalytic reduction method, selective non-catalytic reduction method, nano catalyst, ozone injection, etc. Although these methods are effective, they cannot completely remove NO_x. Since nitric oxide (NO) is the main part of NO_x, diagnostic methods need to be adopted to quantify NO concentration and understand NO formation. Although the NO formation in many hydrocarbon fuels has

been quantitatively measured using different diagnostic techniques, e.g. [37-45], there have been zero quantitative measurements of NO mole fraction of DME/air flames in the existing literature, which limits the understanding of NO formation and improvement of the kinetic model of DME flames.

1.3. Scope of this work

From the literature survey, it is evident that the experimental results of laminar burning velocity of DME/air mixtures are significantly scattered, and that there is a lack of data of NO concentration for DME flames. For these reasons, it is important to gain insights into the fundamental combustion properties of DME and provide valuable data for modelers to improve chemical kinetic models. Moreover, these experimental data and the derived temperature dependence of burning velocity also play a critical role in the design of practical devices.

Three tasks are involved in this project. The first task is to measure the laminar burning velocities of premixed DME/air mixtures using the heat flux method at standard pressure and different unburned gas temperatures (298-338 K) and derive the temperature dependence. The second task is to measure the NO mole fractions in the post-flame zone of DME/air mixtures preheated at 338 K using laser induced fluorescence (NO-LIF). The last task is to use the experimental data to check the agreement of the existing literature data and to check the performances of six chemical kinetic models available in the literature in predicting the present data.

This thesis is mainly divided into six chapters. After a brief introduction of the motivation and purpose of this project, the theoretical background is introduced in Chapter 2. Then, the heat flux method, the laser-induced fluorescence technique and computational tools applied in this thesis are presented detailly in Chapter 3. Chapter 4 discusses the experimental and simulation results. Finally, conclusions and outlook are drawn in Chapter 5 and Chapter 6.

2. Theoretical Background

2.1. Laminar burning velocity of combustible mixture

2.1.1. Definition

A premixed flame means that the fuel and oxidizer have been thoroughly mixed in the burner before combustion. It has been implemented in laboratories since the 18th century. It is a typical combustion method alternative to a diffusion flame. According to the actual fuel/air ratio of the gas mixture, it is divided into two types: partially premixed combustion and completely premixed combustion. Premixed flames have different laminar burning velocities (S_L) under different equivalence ratios (Φ). As presented in Eq.1, the equivalence ratio is defined as: the ratio of the actual fuel/oxidizer ratio to the stoichiometric fuel/oxidizer ratio [46], where m is the mass of the substance and n is the amount of substance. If $\Phi = 1$, stoichiometric combustion occurs, the generated products are only energy, water and carbon dioxide. If $\Phi < 1$, it is fuel-lean combustion with excess oxidizer. On the contrary, it is fuel-rich combustion with insufficient oxidizer when $\Phi > 1$. For pure oxidizer and pure fuel, the equivalence ratios are $\Phi = 0$ and $\Phi = \infty$, respectively.

$$\Phi = \frac{\left(\frac{Fuel}{Oxidizer}\right)}{\left(\frac{Fuel}{Oxidizer}\right)_{stoichiometric}} = \frac{m_F/m_O}{(m_F/m_O)_{st}} = \frac{n_F/n_O}{(n_F/n_O)_{st}} \quad (1)$$

Laminar burning velocity is the propagation speed of an adiabatic, unstretched, premixed flat flame relative to the incoming unburned premixed gas mixture [47]. It is affected by the type of fuel, equivalence ratio, dilution, temperature, and pressure, and can be approximately predicted by kinetic mechanisms. S_L is an important parameter for determining the heat release rates, explaining combustion phenomena, such as flame stabilization, flashback, and blow off. Therefore, it is widely used to validate chemical kinetic models and provides an important parameter for modeling combustion products and designing practical combustion devices.

2.1.2. Experimental methods

To date, different experimental methods for measuring laminar flame speed of fuel/ oxidizer gas mixtures have been developed by researchers, including stagnation flames, closed vessels, heat flux burners, externally heated diverging channels, and annular stepwise diverging tubes.

2.1.2.1 Stagnation flame method

The stagnation flame method has been widely employed to measure burning velocity at standard ambient temperature and pressure [8-16]. It includes the opposed-jets method and the single-jet method. The configuration of the twin premixed stagnation flame method is shown in Figure 1. It is a method based on the opposed jet stabilization of the fuel/oxidizer mixtures. The fuel and oxidizer are mixed before passing through the nozzles on both sides, and then pass through the nozzles at a certain speed, generating two flames away from the stagnation plane. However, it can be found that the streamlines of the gas flows are not perpendicular to the flame fronts. After the flames meet, a velocity component in the y direction is generated, resulting in a gradual decrease in the flow speed in the x direction. Hence, the flame is stretched because of the velocity gradient along the flame front, i.e. the y direction. In the experiments, the distance between the two nozzles and the flow rate of the premixed gas at the nozzle outlet can be arbitrarily adjusted. Therefore, through adjusting the distance between the nozzles and the flow rate of the premixed unburned gas mixtures at the nozzle outlets to change the stretching rate of the flame, the stretched flame speeds and flame stretching rates can be measured. Then the burning velocity with zero velocity gradient along flame front, y-direction, can be obtained by extrapolation methods. The key benefit of this method is that the flame is not attached to the burner nozzles, thereby avoiding the effect of heat losses. However, van Maaren et al. pointed out that the burning velocity corrected by the linear extrapolation method is overestimated [35].

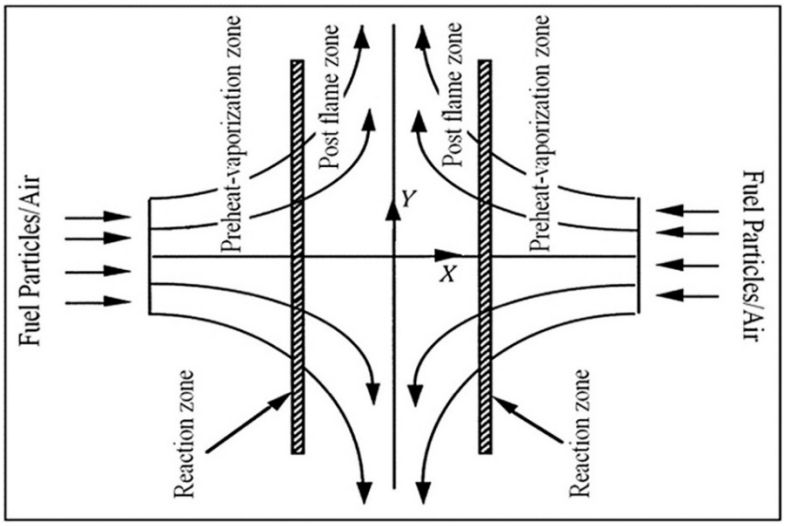

Figure 1: Configuration of twin premixed stagnation flame method, reprinted from reference [48].

2.1.2.2 Spherical flame method

The spherical flame method is another method that obtains the laminar burning velocity by extrapolation. A schematic of the spherical flame method is illustrated in Figure 2. The method consists of adding the fuel/oxidizer mixture into a closed vessel and igniting the gas mixture in the center by an ignition system; then, the flame gradually expands from the center to the surroundings. The flame propagation process can be collected by a high-speed camera, and the flame propagation velocity can be derived from the relationship between time and radius or pressure and time. Since flames generated by this technique is stretched, flame stretching correction is needed so as to obtain the laminar burning velocity. However, during the flame propagation process, the diffusion of the burning gas to the surrounding area will increase the pressure and temperature in the unburned area, causing a pressure-wave reflected from the container wall that in turn affects the flame front and the flame propagation process.

The advantage of the spherical flame method is that the experimental device is simple, the flame propagation process can be record continuously, and that the pressure and temperature range is wide. For the shortcomings, besides the pressure-wave effect from the container wall on the flame front mentioned before, flame stretching correction, radiative heat losses, impact of ignition energy on the initial stage of flame propagation, etc. will become the error sources of this method.

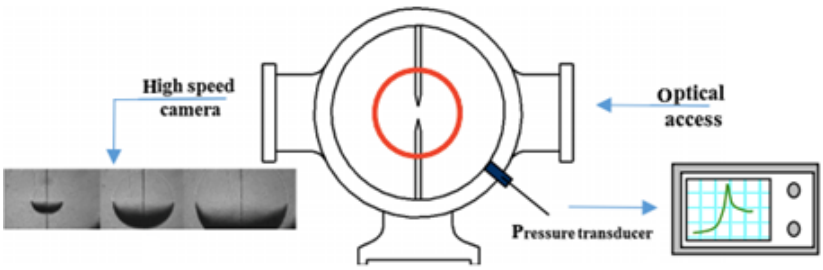

Figure 2: Schematic of the spherical flame method, reprinted from reference [49].

2.1.2.3 Heat flux method

The heat flux method introduced by de Goey et al. [50] in 1993 is a relatively superior method, with which the laminar burning velocity can be obtained directly. In this method, a perforated brass plate was introduced as a burner plate. Due to the special design of the burner plate, which is thin and has multiple small holes forming hexagonal perforations, it forms a flat and non-stretched flame. In addition, the brass plate is surrounded by a hot water bath to preheat the unburned gas mixture. Therefore, when the heat loss needed to stabilize the flame is same as the heat obtained from the brass burner plate, an adiabatic, zero-stretching, one-dimensional, planar flame can be

achieved. Since the adiabatic conditions can actually be generated, and no extrapolation is required to correct flame stretch, the data generated by the heat flux method are very valuable for model validation. Therefore, the heat flux method was employed in the present work. However, one of the shortcomings of this technique is that it only can be implemented in a relatively small pressure and temperature range. The heat flux burner with the current structure can only measure the flame speed up to 70 cm/s [3]. If the flame speed exceeds 70 cm/s, the size of the holes in the burner plate needs to be further reduced, which will increase the difficulty of manufacturing the burner plate. Moreover, the burning velocity can only be measured below 10 atm because at higher pressures the flame becomes difficult to stabilize [3], due to the decrease of the burning velocity with increasing pressure. However, since the present work only focus on the burning velocity at T_g = 298-338 K and P = 1 atm, the heat flux method is sufficient for this study; detailed information about this method will be described in Section 3.1.

2.1.2.4 Externally heated diverging channel method

The externally heated diverging channel method was presented by Akram and Kumar in 2012 [51]. In this method, the burning velocity is derived from the mass conservation at the flame front [3]. A schematic of this technique is presented in Figure 3. Fuel/oxidizer mixtures are fed at the inlet of the channel and ignited at the outlet. The flame is stabilized at a position where the flame speed is the same as the unburned gas speed. The external heating of the channel wall helps stabilize the flame at elevated temperature conditions, and achieves an almost adiabatic flame, i.e. the heat loss from flame to the channel wall can be compensated by the heated channel wall [3]. The flame generated by this technique is also flat, thanks to the special geometry of the channel: a high aspect ratio promotes to form a uniform flow field, and the gradually divergent shape from the inlet to the exit helps to prevent flame flashback [3,18]. Mohammad et al. have studied in detail the effects of aspect ratio of channel, divergence angle, and external heating temperature on laminar flame velocity [52]. In this method, in order to obtain a more accurate experimental data, problems due to heat losses, hydrodynamic stretching, and flame stability still need to be resolved.

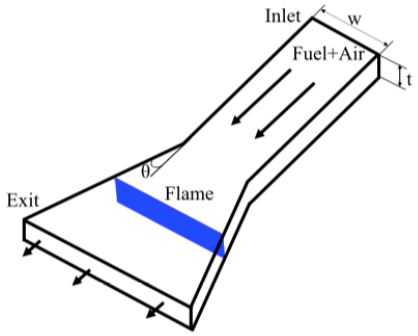

Figure 3: Schematic of externally heated diverging channel method, reprinted from reference [3].

2.1.2.5 Annular stepwise diverging tube method

The annular stepwise diverging tube method (ASDT) proposed by Kim et al. [19,20] is a relatively new method for studying the overall length scale impact on the flame propagation speed in a narrow channel. ASDT with higher experimental resolution is the improvement of the annular diverging tube (ADT). In ADT, a flame is stabilized in a slightly tapered core, see Figure 4 (a). Kim et al. indicated that when the flame shape is least inclined, the critical flow velocity is close to burning velocity [20]. The main difference between ASDT and ADT is the shape of the core. The tapered core is replaced by a stepwise core in ASDT, see Figure 4 (b). In ASDT, consecutive flow divergences is introduced at each step, to form a stable and flat flame in the azimuth direction. Therefore, the flame propagation velocity can be obtained through reading the flame position at fixed flow rates [20].

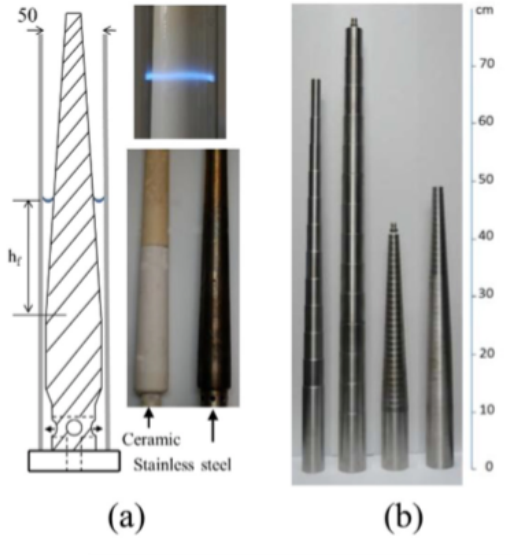

Figure 4: (a) An annular diverging tube method, (b) annular stepwise diverging tubes, reprinted from reference [3].

2.2 Laser-induced fluorescence

Laser-induced fluorescence (LIF) is a measurement method that uses a laser with a certain wavelength to pump atoms or molecules in the ground state to an excited state, and then detects the fluorescence released after the molecules are de-excited to the ground state, see Figure 5. However, when the molecules are de-excited from the excited state to the ground state, most molecules loose energy by collisional quenching and do not emit fluorescence. Therefore, it is difficult to quantify the fluorescence signal induced by the laser into a species concentration, since the number of excited molecules that actually give fluorescence is unknown.

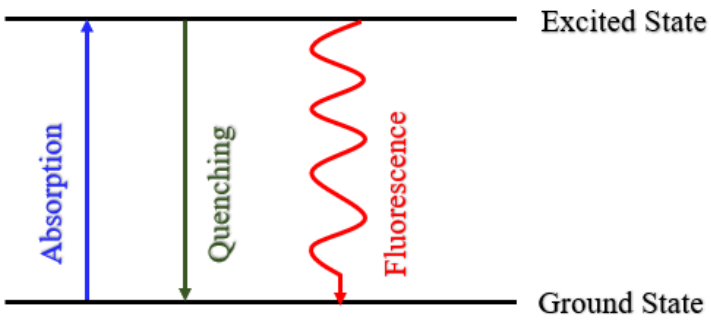

Figure 5: Schematic of the laser induced fluorescence process.

The energy of the photons absorbed and emitted by the molecules is the same as the energy difference between the transition levels, so the wavelength range of the photons absorbed and emitted by substance is well determined. At ambient temperature, as these molecules are at a lower energy level, the wavelength of fluorescence is usually larger than the wavelength of incident light, which is called Stokes Shift. Conversely, if the wavelength of the incident light is greater than the wavelength of the fluorescence, it is named anti-Stokes shift. For the fluorescence phenomenon, once the light irradiation is stopped, the fluorescence process will also stop within a few nanoseconds for measurements in flames.

LIF has the following advantages: first, it has high detection sensitivity; second, non-resonant fluorescence signal helps to remove other stray light with a filter; third, its spectral lines are easy to identify and interpret.

3. Experimental and numerical methods

3.1. Heat flux method

3.1.1. Principle

As described in Section 2.1.2.3, an adiabatic stretchless flat flame can actually be generated in the heat flux method, thus, laminar burning velocity (S_L) can be directly determined without any flame stretch correction in the post processing. Since extrapolation method always has unavoidable errors, heat flux method used in this study shows better performance than stagnation flames and spherically expanding flames that obtain burning velocity by extrapolation method.

The ideal case for finding laminar burning velocity is that the flame should be one-dimensional and as flat as possible [54]. This flame condition is achieved by introducing a burner that stabilizes a flame on a very thin brass plate with multiple small holes forming hexagonal perforations, see Figure 6. The relation between the temperature distribution and radius on the burner plate is:

$$T(r) = T_0 - \frac{q}{4\lambda h} r^2 \tag{2}$$

where T_0 represents the temperature at the center point, T(r) is the temperature at a radius r from the center point, h is the thickness of the burner plate, λ is the thermal conductivity of the brass burner plate in radial direction, and q is net heat transfer that is the difference between the heat gain (q^+) and heat loss (q^-), i.e. :

$$q = q^+ - q^- \tag{3}$$

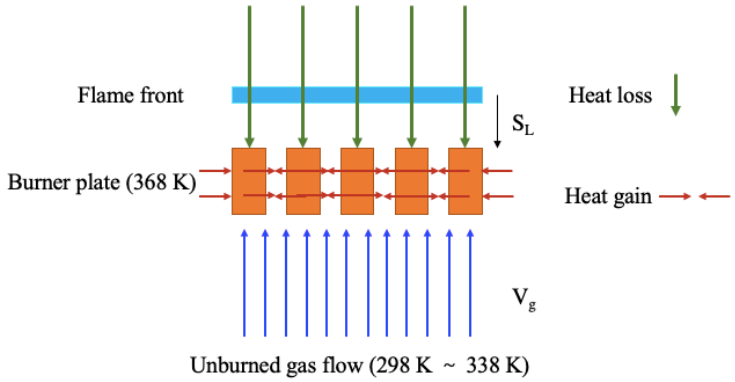

Figure 6: Scheme of heat flow transfer.

As illustrated in Figure 6, the horizontal arrows indicate the heat gain (q^+) of the initial gas mixture from the burner plate which is heated by a hot water circuit located in the outer layer of the burner plate and maintained at a temperature of 368 K, and the vertical downward arrows represent the heat lost (q^-) from the flame to the burner plate to stabilize a flame. $\frac{q}{4\lambda h}$ is the parabolic factor, denoted as C, which can be obtained by fitting to Eq. 2, and depends on the unburned mixed gas velocity V_g, V_g is defined as:

$$V_g = \frac{P_0}{P} \cdot \frac{T_g}{T_0} \cdot \frac{F_{tot}}{A} \quad (4)$$

where F_{tot} is the total flow rate, A is the perforated area of the burner plate, P is the pressure during the experiment, T_g is the initial gas temperature, and T_0 and P_0 are ambient temperature and standard pressure, respectively.

The temperature distribution measured by thermocouples at different radius of the burner plate varies with the change of the unburned gas velocity V_g. It means that changing the entering initial gas velocity, V_g, the net heat q and parabolic factor C will be affected. When $q = 0$, it means that the heat lost for stabilizing the flame is same as the heat gained by the unburned gas mixtures when passing through burner plate, and the flame reaches adiabatic conditions. Then C = 0 and the temperature profile becomes flat (see Eq. 2), in this case, the laminar burning velocity S_L is equal to the unburned gas velocity V_g. Moreover, when $V_g > S_L$ and C > 0, it is named a super-adiabatic state, in this case the heat gain obtained from water bath is not sufficient to compensate for the heat loss needed to stabilize the flame, leading to a decrease in temperature of the center of the burner plate. If the gas velocity is much larger than the flame speed, the flame will eventually blow off [55]. On the contrary, when $V_g < S_L$ and C < 0, it is called a sub-adiabatic state. In this technique, S_L is usually obtained by interpolating the burning velocities measured under super-adiabatic and sub-adiabatic states. However, when the experiment is carried out at relatively high temperatures, flame corrugation or cell formation may be formed at super-adiabatic conditions. In this case, S_L is obtained by extrapolation from sub-adiabatic condition to adiabatic conditions. It is worth noting that the velocity range used for extrapolation should not be too large, otherwise the $C(V_g)$ profile becomes non-linear and the flame will be closer to the burner, causing an increase in temperature of the burner plate. For the non-linear effects on $C(V_g)$, the normalized coefficient method, $c_r = C/V_g$, presented by Alekseev et al. [47], can be employed to reduce the nonlinear effect. Two data interpolation methods were used in the experimental data processing, and it was found that the difference in obtained S_L was similar. Because the flame cannot reach the adiabatic state under high temperature and high flow rate conditions, all S_L in this project were obtained using the normalized coefficient method.

3.1.2. Experimental setup

As shown in Figure 7, the experimental setup for the S_L measurement of premixed DME/air mixtures is divided into two parts: 1. Gas feeding system; 2. Heat flux burner system.

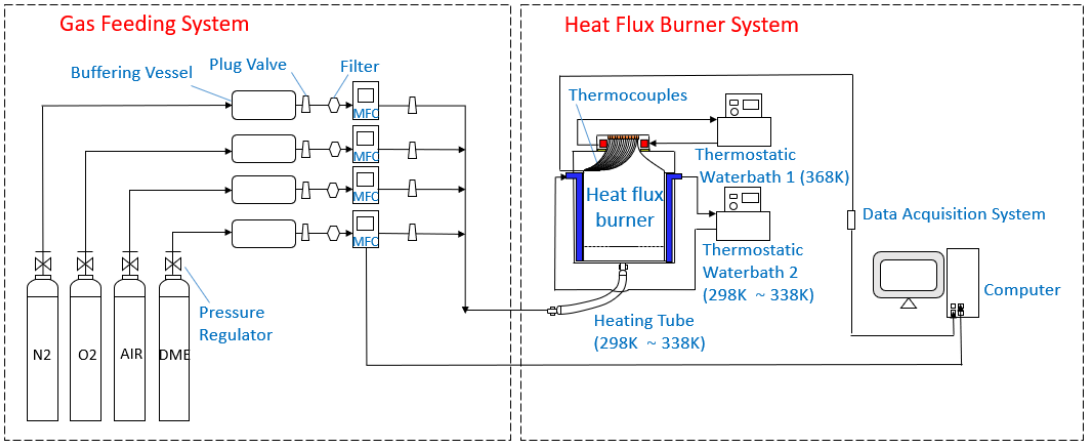

Figure 7: Schematic of the experimental setup for laminar burning velocity measurement.

3.1.2.1 Gas feeding system

The gases come from a central supply system or fuel tanks in the laboratory. The purity of DME, O_2 and N_2 used in these experiments was 99.9%. The composition of air is 21% O_2, 79% N_2, 1% relative uncertainty. In S_L measurements, only DME and air were employed. N_2 and O_2 were used for NO calibration in the NO-LIF part. The role of the buffering vessels is to suppress fluctuations in the inlet flow. Filters placed before each mass flow controller (MFC) are employed to remove impurities in the gas flow. The pipeline between buffering vessels and MFCs is surrounded by a hose filled with hot water (398 K) to prevent DME condensation. MFCs connected to the computer can accurately control or measure the mass flow of the gas through a LabVIEW interface to achieve the wanted equivalence ratio. Generally, the flow rates set by MFCs are different from the actual flow rates, because of the uncertainty of the MFC components. Therefore, MFCs need to be calibrated before measurements. In this project, MFCs for DME, O_2, N_2 and air were calibrated employing a positive displacement flow meter (MesaLabs Definer 220). For the calibration process, firstly, the flow rates were set as 0.05, 0.1, 0.2, 0.3, 0.4, 0.5, 0.6, 0.7, 0.8, 0.9, 1.0 times of the capacities of MFCs, see Table 1, and data were recorded after the flow rates reached a steady state. Secondly, the obtained flow rates and the set flow rates were fitted by fourth-order polynomials

in forward and backward directions, respectively. Finally, the coefficients were inserted into the LabVIEW script before starting the experiments.

Plug valves are installed to make sure that the flow can be manually closed when the MFCs lose control. If a line is not in use, the valves on it are closed. When the gas flows leave the MFCs, they are fully mixed in the pipe and then enter the burner.

Table 1: MFCs used in the experiments.

	Manufacturer	Maximum capacity (L/h)	Gas
MFC1	Bronkhorst High-Tech B.V.	30	Air
MFC2	Bronkhorst High-Tech B.V.	10	N_2
MFC3	Bronkhorst High-Tech B.V.	10	O_2
MFC4	Bronkhorst High-Tech B.V.	4	DME

3.1.2.2 Heat flux burner system

The core of the laminar burning velocity measurement is the heat flux burner, which includes a burner head, a plenum chamber, and a perforated plate, whose radial temperature distribution is measured by 15 E-Type thermocouples attached on it. This burner designed by Eindhoven University of Technology is used to investigate the S_L of fuel/oxidizer mixtures under different conditions, such as temperature, fuel/air ratio, and dilution concentration [56]. The structure diagram is shown in Figure 8. Each part of the heat flux burner will be introduced in the following sections.

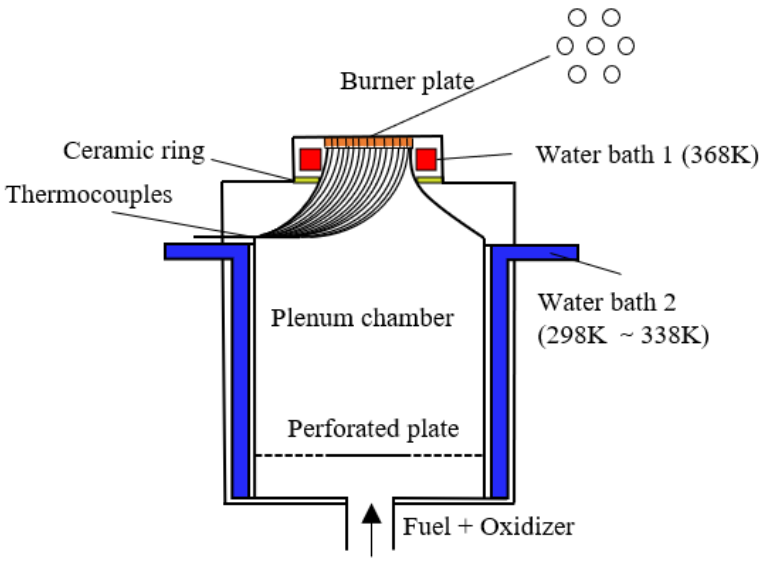

Figure 8: Scheme of the heat flux burner.

3.1.2.2.1 Burner head

As illustrated in Figure 8, the shape of the burner head gradually converges from bottom to top, which helps to generate a uniform flow. The thermostatic water bath 1 (Grant Instrument, model GD120) with dual water circuit is set to 368 K to compensate for the heat loss needed to stabilize the flame. As shown in Figure 9 (b), the two water circuits are installed around the burner plate and the bottom of burner head, respectively, to effectively maintain the burner plate at 368 K and stabilize the flame. An insulated ceramic ring is installed between the burner head and plenum chamber, see Figure 9 (a). Due to its low thermal conductivity, the heat flux burner is divided into a hot part and a cold part. In addition, the ceramic ring has the following advantages: first, the heat loss from the burner head to the plenum chamber can be effectively reduced, thus, less water flow is required to maintain the plenum chamber at ambient temperature; second, because less heat is transferred to the plenum chamber, the burner head can reach steady state faster; third, the ceramic ring can reduce the flame boundary effect, since the heat transfer from the burner head to the unburned gas mixture occurs only in places where there is a temperature difference [54].

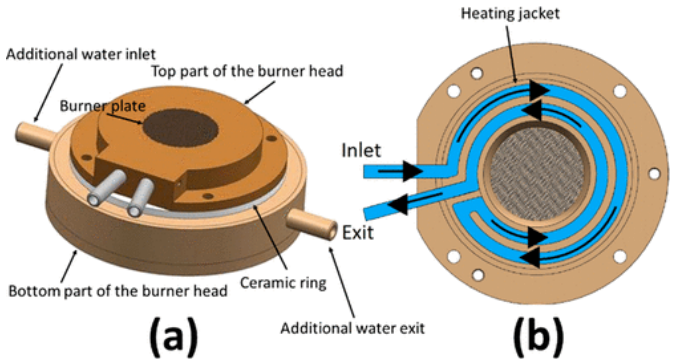

Figure 9: (a) Burner head, (b) Dual water circuit system, reprinted from reference [56].

3.1.2.2.2 Plenum chamber

The gas mixture from the outlet of MFCs enters the plenum chamber of the heat flux burner through a heating tube that prevents condensation. After gas mixtures enter the plenum chamber, there is a perforated plate with a solid center and perforated edges installed in the lower part of the plenum chamber to distribute the incoming gas flow, see Figure 8.

The function of the plenum chamber is to control the temperature of initial gas mixtures and to produce a uniform flow before entering the burner plate. It is surrounded by a thermostatic water bath 2 (Grant Instrument, model GD120) to control the temperature of the initial gas mixtures T_g at 298 K, 308 K, 323 K, 338 K in this

project. In addition, water bath 2 is an important part to stabilize the unburned gas mixtures. Without this water jacket, the unburned gas mixture will absorb heat from the perforated plate and plenum chamber wall heated by the burner head, resulting in a change in the temperature of the unburned gas mixtures.

3.1.2.2.3 Burner plate

The burner plate with a thickness of 2 mm and a radius of 15 mm is made of brass. It has multiple hexagonal perforated holes with a radius of 0.2 mm, a spacing of 0.47 mm between the holes, and a perforation area of 6.9004 cm^2. In addition, 15 E-type thermocouples with a radius of 0.038 mm are inserted into holes for temperature monitoring. These characteristics of the burner plate ensure that the flame is stable, flat and 1-D.

3.1.3. Validation of experimental methodology

Before measuring the laminar burning velocity of DME, it was necessary to use methane (CH_4) as a reference fuel to validate the feasibility of the experimental methodology and experimental setups. As presented in Figure 10, the difference between the measured burning velocity and the reference burning velocity provided by Lubrano Lavadera et al. [56] on the same heat flux burner does not exceed 1 cm/s, which proves the feasibility of the experimental methodology and setup.

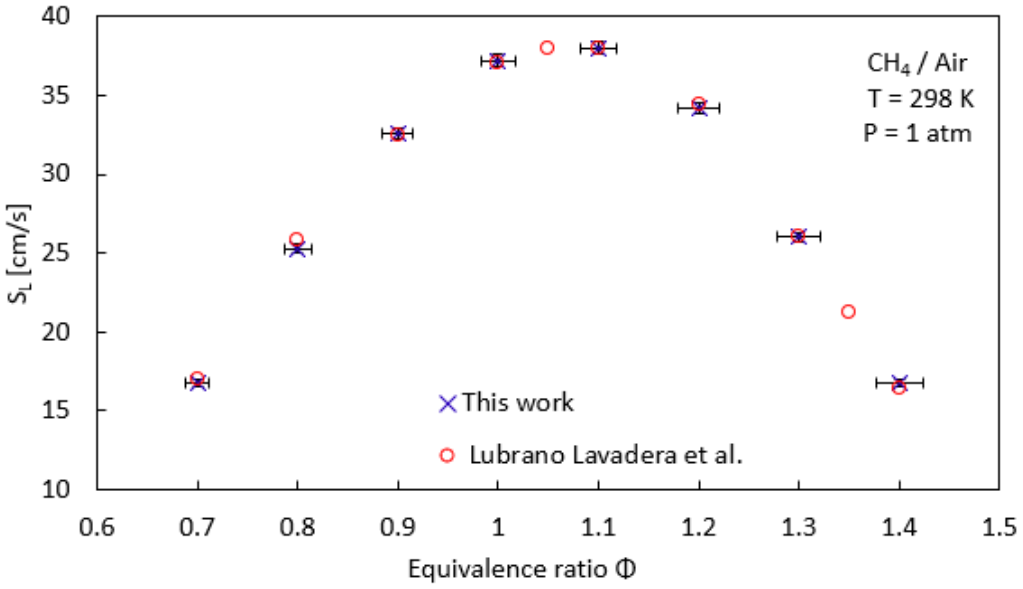

Figure 10: Laminar burning velocity of CH_4 /air mixtures at standard ambient temperature and pressure.

3.1.4. Experimental Uncertainties

Alekseev et al. [47] reported in detail several uncertainties in S_L measurement by the heat flux method, such as fuel and gas purity, composition, scatter in thermocouple readings, uncertainty in MFCs, cell formation, initial gas mixture temperature, perforation of holes, atmospheric pressure variations, etc., see Table 2.

Table 2: Uncertainty factors in S_L measurement, cited from reference [3].

Factor	ΔS_L	Method to control/ Investigate
MFC	~1%	Calibration of Mass Flow Controller
Mixing	<0.15 cm/s	Heating hose, long tube
T_g	0.3–2%	TC in the flow
P	~1%	Record pressure in the room
V_g uniformity	~0.5%	Change the diameter of the burner
Perforation	~0.5%	CFD simulation
Radiation	<0.5 cm/s	Kinetic modelling
Asymmetric heating	Up to 2–3 cm/s	Check the symmetry of TC readings

Since a new burner with improved burner head was used in this experiment, the uncertainty in S_L is only 0.2-0.5 cm/s [56]. The total uncertainty in S_L mainly comes from two factors: scatter in thermocouple readings and uncertainty in MFCs.

Alekseev et al. [47] gave the uncertainty in S_L caused by the thermocouple readings as

$$\Delta S_L^{TC} = \frac{1}{s}\frac{2\sigma_{TC}}{r_b^2} \tag{5}$$

where σ_{TC} is the thermocouple accuracy, r_b is the radial position of the outmost thermocouple, and s expressed in equation 6 is the parabolic coefficient sensitivity under adiabatic flames, i.e. the slope of the $C\ (V_g)$ curve at $V_g = S_L$.

$$S = \left.\frac{dC}{dV_g}\right|_{V_g=S_L} \tag{6}$$

In addition, for a gas mixture formed with single-fuel and single-oxidizer, the uncertainty in burning velocity resulted from the flow rate measurement is

$$\Delta S_L^{MFC} = S_L \frac{\Delta F_{tot}}{F_{tot}} = S_L \frac{\sqrt{\Delta F_{fuel}^2 + \Delta F_{oxidizer}^2}}{F_{tot}} \tag{7}$$

where ΔF_{tot} is the uncertainty resulted from the total flow rate F_{tot}, while ΔF_{fuel} and $\Delta F_{oxidizer}$ are the uncertainties caused by the flow rates of fuel and oxidizer,

respectively. As mentioned before, MFCs must be calibrated by a flow meter before measurements. Therefore, the uncertainty in the flow rate of fuel, ΔF_{fuel}, or oxidizer, $\Delta F_{oxidizer}$, is a sum of the stated accuracy of the flow meter 1% and the stated flow repeatability of the MFCs 0.2% [47]. They are expressed as

$$\Delta F_{fuel} = \pm 1.2\%\ F_{fuel} \tag{8}$$

$$\Delta F_{oxidizer} = \pm 1.2\%\ F_{oxidizer} \tag{9}$$

Moreover, the uncertainty in equivalence ratio Φ is defined as

$$\Delta\Phi = \Phi\sqrt{(\frac{\Delta F_{fuel}}{F_{fuel}})^2 + (\frac{\Delta F_{oxidizer}}{F_{oxidizer}})^2} \tag{10}$$

Thus, the relationship between Φ and $\Delta\Phi$ is

$$\Delta\Phi = 1.7\%\ \Phi \tag{11}$$

In summary, the total uncertainty in S_L is a sum of ΔS_L^{TC} and ΔS_L^{MFC}, and the uncertainty in Φ is 1.7%.

3.1.5. Extraction of the temperature dependence of S_L

In practical situations, mixtures are usually burned under elevated temperature conditions. Therefore, S_L is usually measured at different temperatures and pressures. The relationship between them is

$$S_L = S_{L,0}(\frac{T_g}{T_0})^{\alpha}(\frac{P}{P_0})^{\beta} \tag{12}$$

where T_g and P represent the temperature and pressure of the initial gas mixtures, T_0 and P_0 denote the temperature and pressure at reference conditions. $S_{L,0}$ is the reference laminar burning velocity. α and β are the power exponents of temperatures and pressures, respectively, and they depend on the equivalence ratio. In this project, only initial gas temperatures T_g were changed, pressure remained the same, $P = P_0 = 1$ atm. Eq. 12 can be simplified as

$$S_L = S_{L,0}(\frac{T_g}{T_0})^{\alpha} \tag{13}$$

Therefore, the temperature dependence α can be determined by calculating the slope of the linear relationship between $\frac{S_L}{S_{L,0}}$ and $\frac{T_g}{T_0}$ on a log-log scale. If burning velocity at several initial mixture temperatures are studied, the expression of α is:

$$\alpha = \frac{\sum_i lnS_L^{T_i} ln\frac{T_i}{T_0} - \frac{1}{n}\sum_i ln\frac{T_i}{T_0}\sum_i lnS_L^{T_i}}{\sum_i ln^2\frac{T_i}{T_0} - \frac{1}{n}(\sum_i ln\frac{T_i}{T_0})^2} \tag{14}$$

where n is the number of measured temperatures and $S_L^{T_i}$ is the flame speed at initial mixture temperature T_i.

For a known fuel/oxidizer mixture, α is also related to the equivalence ratio, mixture concentration, diluent composition, and measured temperature range [47]. The role of α is to evaluate the S_L at higher temperatures for the design of practical applications and to provide a stringent test for the validation of literature chemical kinetic models. In this project, α is determined from experimental results and models available in literature.

According to Alekseev et al. [47], the uncertainty in α resulting from $\Delta S_L^{T_i}$ can be estimated by using the error propagation rule on equation 14:

$$\Delta\alpha = \frac{(\sum_i[(ln\frac{T_i}{T_0} - \overline{ln\frac{T_i}{T_0}})\cdot\frac{\Delta S_L^{T_i}}{S_L^{T_i}}]^2)^{0.5}}{\sum_i ln^2\frac{T_i}{T_0} - n\cdot(\overline{ln\frac{T_i}{T_0}})^2} \tag{15}$$

where $\Delta S_L^{T_i}$ the uncertainty of flame speed at initial gas mixture temperature T_i, and $\overline{ln\frac{T_i}{T_0}}$ is the mean logarithmic normalized temperature:

$$\overline{ln\frac{T_i}{T_0}} = \frac{\sum_i ln\frac{T_i}{T_0}}{n} \tag{16}$$

3.2. Laser induced fluorescence of nitric oxide

As nitric oxide (NO) is a very important combustion pollutant, quantitative and qualitative measurements of NO concentration are important for reducing air pollution. One problem with quantitative measurement of NO concentration is that although the laser irradiance is high enough to reach saturated fluorescence conditions, the fluorescence signal is still affected by rotational-energy transfer (RET) and collisional

quenching [45]. However, Brackmann et al. [45] mentioned that the NO-LIF signal could be converted into NO mole fraction by NO calibration.

A new LIF installation with new mirrors combination and stabilizer was given by Brackmann et al. [45] and employed in this study to measure the NO mole fraction in a premixed DME/air flame 1 cm above the burner plate at atmospheric pressure and 338 K. The NO concentration is quantified through a NO calibration process, which is achieved by seeding different NO mole fractions (ppm) in a lean flame. This LIF technique has been successfully implemented in premixed CH_4/air flames and CH_3OH/air flames [45], and the experimental results showed very good agreement with different chemical kinetic models. In addition, compared with the NO concentration measurements by intrusive probe samplings in CH_4/air flames and CH_3OH/air flames, data obtained by the non-intrusive LIF technique showed better performances [45]. Since introducing a probe into the flame will lower the temperature, resulting in a decrease in the formation of thermal NO around stoichiometric conditions. Moreover, compared with other conditions, the flame is less stable in the fuel-rich conditions. Therefore, the probe sampling will affect the flame stability more.

The NO transition studied in this project is shown in Figure 11, NO molecules are excited from v'' = 0 of electronic energy level $X^2\Pi$ to v' = 0 of electronic energy level $A^2\Sigma^+$ on the transition line Q_2 (26.5) by a laser beam operated at 225.5 nm. The reason for using transition line Q_2 (26.5) is that the population of the J = 26.5 level, given by the Boltzmann distribution, is insensitive to temperature changes and the NO signal is much higher than the background at this line, i.e. high signal to background ratio; and there are few absorption lines in this band, only NO and O_2, otherwise the spectrum will be interfered. Since the excited molecules cannot stay in an excited state for a long time, a de-excitation process occurs. The molecules are released from v' = 0 of the electronic energy level $A^2\Sigma^+$ to v'' = 2 of the electronic energy level $X^2\Pi$, thereby generating fluorescence with a wavelength centered at 247 nm.

Brackmann et al. [45] mentioned that the NO-LIF employed in this experimental setup is a broadband detection of the entire vibration band, thus, the fluorescence can come from all rotational energy levels, and the impact of the rotational energy transfer (RET) cannot be ignored. Moreover, the emission from non-laser-excited rotational energy levels is not stimulated by the laser but fluorescence and collisional quenching. Therefore, the effects of RET and collisional quenching should be considered in data processing.

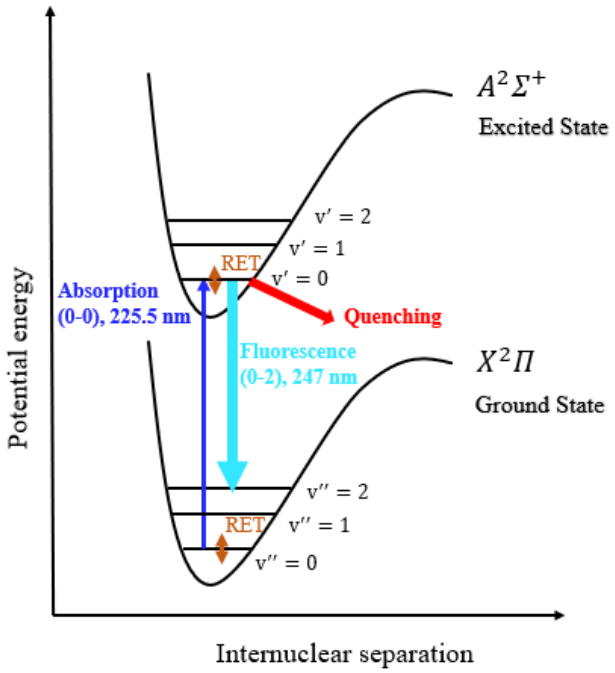

Figure 11: Energy level diagram showing the NO transitions in this experiment.

3.2.1. Laser-induced saturated fluorescence

Laser-induced saturated fluorescence (LSF) is based on using high-power density excitation lasers to achieve saturated or near-saturated optical transitions [60]. The advantage of LSF is that the generated LIF signal is independent on the collisional quenching and laser intensity fluctuations, as shown in the Figure 12. Since when the laser irradiance is low, it has a linear relationship with NO signal. And when LIF excitation is in linear regime, the fluorescence field is affected by the non-radiative de-excitation generated by collisional quenching, which causes difficulties in quantification of LIF [45]. When the irradiance gradually increases, the signal still increases with the increase of irradiance, but it no longer has a linear relationship and reaches an incomplete saturation state, due to that the irradiance in ‘wings’ of the spatial laser profile is very low. With the further increase in irradiance, the "wing" also reached saturation condition, and the NO signal is insensitive of the laser irradiance, reaching a saturated LIF, which could reduce the impact of the collisional quenching effect. To reduce the collisional quenching effect, the pulse energy used in this project was 2.0-2.5 mJ.

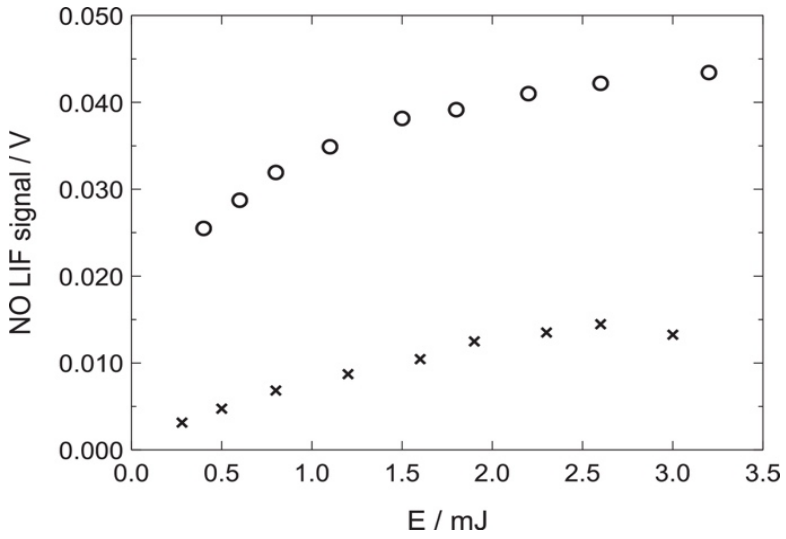

Figure 12： The relationship between NO-LIF signal and laser pulse energy, reprinted from reference [45]. (circles: resonance-on, crosses: resonance-off)

3.2.2. NO calibration procedure

The NO-LIF signal can be converted to NO mole fraction by calibration [45]. Calibration is achieved by seeding different NO mole fractions (ppm) in a lean flame where the native NO concentration is very low. As presented in Figure 13, Brackmann et al. showed that there is a linear relationship between the NO seeding with different mole fractions and the obtained NO-LIF signal in methane, syngas, and methanol flames. In addition, the higher slope of syngas compared to that of methane is due to the fact that temperature of syngas (1543 K) is lower than that of methane (1785 K) and the presence of NO reburning in methane. Therefore, syngas was used as the calibration flame in the experiments of Brackmann et al.

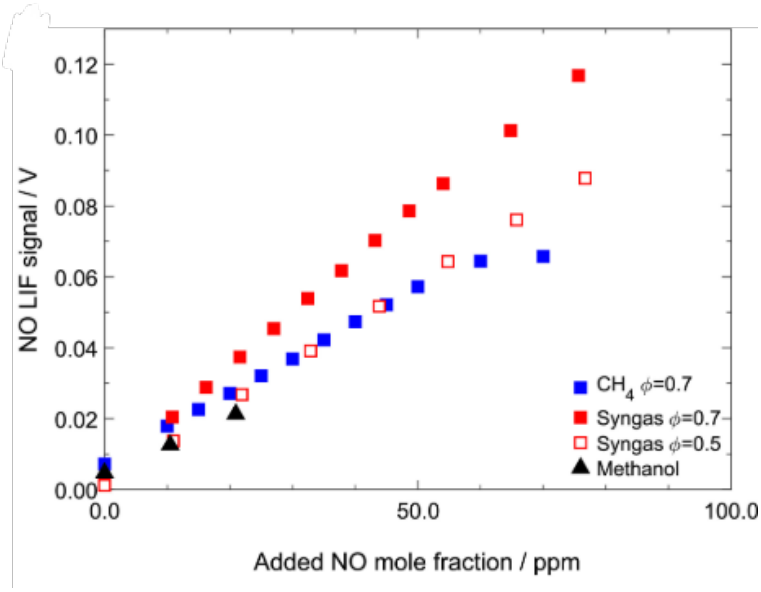

Figure 13: Relationship between NO-LIF signal and NO seeding with different mole fraction of methane, syngas and methanol flames at $\Phi = 0.7$ and a syngas flame at $\Phi = 0.5$, reprinted from reference [45].

As mentioned before, in the NO calibration measurement, seeded NO mole fraction has a linear relationship with the NO-LIF signal, it can be expressed as

$$F_{flame} = C \times N_{ppm,\ seeded} \tag{17}$$

where $N_{ppm,\ seeded}$ is the seeded NO mole fraction in ppm which is relative to temperature and collisional quenching of the calibration flame; F_{flame} is the fluorescence signal read from digital oscilloscope, and each data point was averaged over 128 laser pulses. C is the slope of the NO-LIF signal as a function of NO seeding concentration, and the slope represents the NO-LIF signal for each NO molecule.

However, since syngas was unavailable in the experiment, the calibration factor for the LSF measurement was determined by seeding 10, 20, 30, 40, 50, 60, 70 ppm NO respectively to a premixed CH_4/air flame at $\Phi = 0.7$, and the laser beam was focused at 1 cm above the burner plate. The relationship between calibration coefficient of syngas and methane is [45]:

$$C_{syngas} = C_{methane} \times 1.157381 \tag{18}$$

where $C_{methane}$ is the slope of the NO-LIF signal versus NO seeding concentration in methane flames, which is equal to 0.0011, see Figure 14. The slope obtained in present work is slightly higher than the one measured by Brackmann et al. [45], $C_{methane} = 0.001035$, this is because the mirrors combination in the front of the spectrometer was

replaced, a stabilizer was added to make the laser more stable, and the collected fluorescence wavelength was changed to a higher peak.

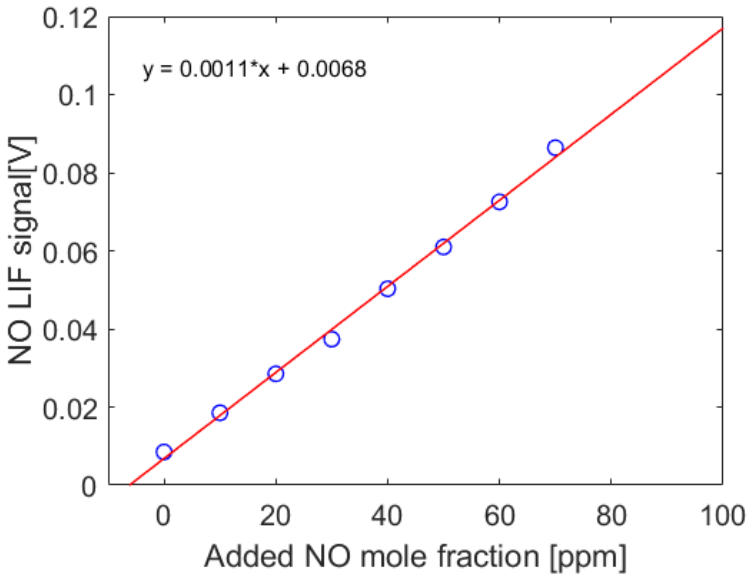

Figure 14: NO calibration in methane flames.

Since the fluorescence field described above is affected by temperature and collisional quenching rate, NO absolute concentration expressed in ppm is

$$N_{ppm,\ abs} = \left(\frac{T_{flame}}{T_{cal}}\right)\left(\frac{f_{cal}}{f_{flame}}\right)\left(\frac{Q_{flame}}{Q_{cal}}\right)N_{ppm,\ seeded}$$

$$= \frac{F_{flame}}{C}\left(\frac{T_{flame}}{T_{cal}}\right)\left(\frac{f_{cal}}{f_{flame}}\right)\left(\frac{Q_{flame}}{Q_{cal}}\right) \quad (19)$$

where T, f, and Q represent flame temperature, Boltzmann fraction, and collisional quenching rate, respectively. The subscript flame and cal indicate the investigated flame and the calibration flame, respectively. Flame temperature T at a height of 1 cm above the burner plate comes from parameter analysis in simulation results which include radiative heat loss. The Boltzmann fraction f can be obtained from the LIFBASE software. In addition, the collisional quenching rate Q is obtained by the combination of the concentration of N_2, O_2, H_2O, CO_2, H_2, and CO provided in parameter analysis of simulation results and the collisional quenching cross-sectional area calculation provided by Settersten et al. [57].

3.2.3. Experimental setup

The schematic of the experimental setup of NO-LIF is presented in Figure 15. It consists of a laser system, an optical system, a heat flux burner system, and a detection system.

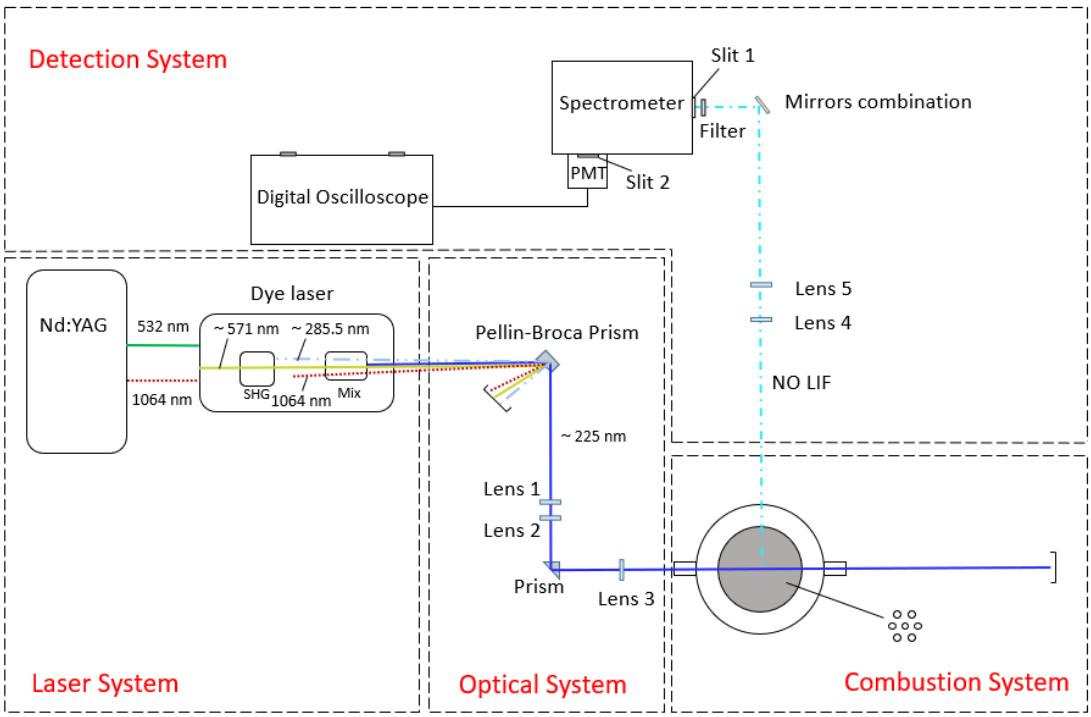

Figure 15: Top view of NO-LIF set up.

The laser system consists of a Nd: YAG laser (Brilliant B, Quantel) and a dye laser (Quantel TDL-90) running on a Rhodamine 590/610 dye mixture. The second harmonic of the Nd: YAG laser at wavelength 532 nm was employed to pump the dye laser, then the output beam at around 571 nm was converted by a frequency-doubling crystal and frequency-mixing crystal. The frequency-doubled dye laser beam was mixed with the fundamental beam of the Nd:YAG laser at 1064 nm, producing a laser beam operated at 225.5 nm on the transition line Q_2 (26.5) in the (0-0) vibration band of the $A^2\Sigma^+ \leftarrow X^2\Pi$ NO transition. The spectral linewidth of the UV beam used to excite the NO molecules is 1 cm^{-1} which depends on the linewidth of the Nd:YAG laser. The laser power was set to around 21-23 mW by adjusting the crystal angle before the experiment.

The optical system consists of a Pellin-Broca prism, a telescope arranged with lens, a prism and a focusing lens. The role of the Pellin-Broca prism is to disperse the 225.5 nm UV light needed for exciting the NO molecules from laser beams of other wavelengths, 1064, 571, 285.5 nm. A telescope, lens 1 and lens 2, with focal length $f = -150$ mm and $f = +300$ mm was used to expand the UV beam, resulting in a smaller focus in the flame. A prism and a focusing lens 3 with focal length $f = +500$ mm located in front of the burner to ensure that the laser beam was focused and can pass through the flame at a height of 1 cm above the burner plate.

The heat flux burner system has been described in the 3.1.2 section, and the detailed experimental setup diagram is shown in Figure 7.

In the collection system, the NO-LIF signal was collected at 90° to the laser beam direction, and focused by lens 4 and lens 5, $\mathrm{f} = +150\,\mathrm{mm}$ and $\mathrm{f} = +300\,\mathrm{mm}$, onto two aluminum mirrors. The role of the two mirrors is to convert the fluorescence signal in the horizontal direction to the vertical direction which is same as the slit of the spectrometer (Shamrock SR-500I-A-R, Andor). In order to remove background, such as flame light and laser, a filter (LP02-224R-25, Semrock) was placed at the entrance of the spectrometer. There are two slits, at the entrance and exit of the spectrometer. The slit 1 at the entrance was used to collect the fluorescence signal reflected from the mirrors. The slit 2 at the exit further selected and outputted the fluorescence spectrum centered at 247 nm in γ (0-2) vibration band of the $A^2\Sigma^+ \rightarrow X^2\Pi$ NO transition to the followed photomultiplier tube (model H9305-01, Hamamatsu). The photomultiplier tube worked at 0.5 V voltage and was placed at the exit of the spectrometer to convert fluorescence signals into electrical signals displayed on a digital oscilloscope (Wavejet Touch 354, Lecroy). Each data point was averaged 128 laser pulse three times. In addition, NO concentration quantification is affected by other background light. O_2, for example, has similar absorption line as NO. Although the overlapped range of absorption line of O_2 and NO is not very large, it still has an impact on measurements in lean flame. Therefore, the laser wavelength was turned to 225.13 nm, where the NO resonance is off, to measure the background. Then the final signal is

$$Signal_{final} = Signal_{NO\ resonance\ on} - Signal_{NO\ resonance\ off} \qquad (20)$$

3.2.4. Experimental uncertainties

For the uncertainties in this methodology, Brackmann et al. calculated the data difference between methane and syngas after flame temperature and quenching correction and found that the error is 8.7%, which includes temperature difference between experimental and calculated temperatures, Boltzmann fraction error and collisional quenching rate error caused by temperature error [45]. Uncertainties due to differences in RET are also expected to be within this range.

3.3. Chemical kinetic modelling

Chemical kinetics is a branch of chemistry. Phenomena like ignition, extinction, and quenching of flames are mainly affected by chemical kinetics.

A well-modeled chemical kinetic model is composed of multiple species and reactions, and each reaction has its own reaction rate. Since the rate parameters are obtained through experimental results or theoretical calculations, they have uncertainties, which will cause a deviation between the simulation results and the experimental values. In recent years, experimental parameters such as laminar burning

velocity and extinction strain rates are usually used to validate and optimize the kinetic models [58].

In order to validate kinetic models of DME from the perspective of laminar burning velocities, the one-dimensional FreeFlame model in ANSYS CHEMKIN 17.0 was used to numerically simulate the experimental results using existing models. Six chemical kinetic mechanisms were implemented in this work to compare simulations with present experimental data and literature data, namely, Konnov 2019 [25], AramcoMech 1.3 2013 [21], Wang 2015 [22], Zhao 2008 [23], POLIMI CRECK 2020 [29,30] with added NO sub-model 2019 [28] and DME sub-model 2015 [26,27], and San Diego with added hydrocarbon model 2016, NO sub-model 2004 and DME sub-model 2015 [24]. The detailed information of these mechanisms is listed in Table 3.

Table 3: Detailed information of employed mechanisms.

Kinetic Mechanism	Species	Reactions	Target
Zhao et al. 2008 [23]	55	290	S_L
Wang et al. 2015 [22]	56	301	S_L
AramcoMech 1.3 2013 [21]	253	1542	S_L
Konnov et al. 2019 [25]	201	2300	S_L + NO formation
POLIMI CRECK [26-30]	316	8418	S_L + NO formation
San Diego [24]	76	337	S_L + NO formation

For all mechanisms, the pressure was set at 1 atm, and the temperatures of the initial gas mixture T_g were set to 298 K, 308 K, 323 K, and 338 K. Thermal diffusion and multicomponent diffusion were included in all simulations. Otherwise, a deviation of 1-2 cm/s may be introduced into the simulation results of S_L [59]. Especially, since radiative heat losses play an important role in thermal NO formation, they are included in the simulation of San Diego, Polimi Creck, Konnov models as well. Additionally, the adaptive grid control based on solution gradient (GRAD) was set as 0.02, the number of adaptive grid points (NADP) was set to 50, and the adaptive grid control based on solution curvature (CURV) was 0.05. These settings cause the grid points to be in the range of 500-1000, thus ensuring that the simulation results are irrelated to the grid.

4. Result and Discussion

In this chapter, the collected literature data, experimental and simulation results will be presented. The experimental results are divided into two parts: laminar burning velocities of DME flames measured from 298 K to 338 K and NO concentration measured in the post-flame zone by the LIF technique at 338 K. By measuring the flame speeds of DME at different temperatures, the exponent α that expresses the dependence of burning velocity on temperature can be derived. Since these experimental data were obtained under adiabatic flame conditions and with a non-invasive flame diagnostic method, they can be regard as highly valuable input for chemical kinetic model validation.

4.1. Laminar burning velocity of DME / air mixtures at ambient temperature

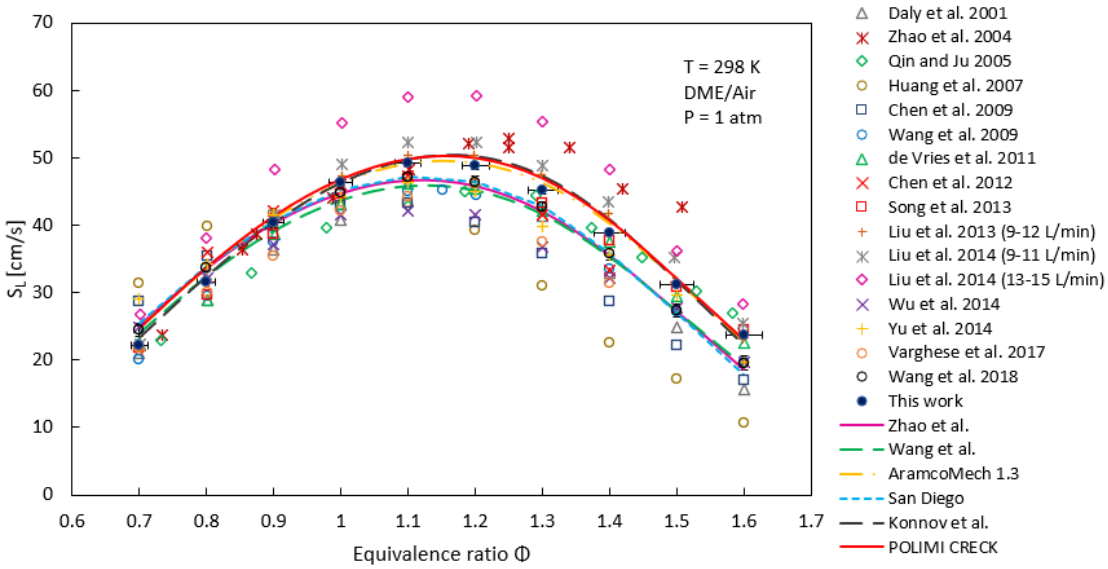

Figure 16: Validation of laminar burning velocity for six mechanisms with data measured in this work and literature data at standard ambient temperature and pressure.

Since the study of laminar burning velocity of the DME/air gas mixtures at P = 1 atm and T_g = 298 K has attracted much attention, in addition to experimental data obtained from this work, Figure 16 also contains six kinetic mechanisms simulation results and a large amount of existing literature data [6-20].

The experimental methods used to measure these S_L data are listed in Table 4. It is easy to find that these literature data are scattered, caused by different experimental methods, equipment, data processing, etc. In the fuel-lean conditions, the scatter between Huang et al. 2007 and Wang et al. 2009 is about 60%. Additionally, data in fuel-rich conditions are more scattered than the data obtained in fuel-lean conditions.

Data obtained in the current study have a good consistency with several literature data [8, 11, 17-20] in fuel-lean conditions, while for fuel-rich combustion, the measured burning velocities are higher than most literature data, as predicted by the Konnov et al., POLIMI CRECK, and AramcoMech 1.3 mechanisms.

Table 4: Different experimental methods used in S_L measurements of DME at standard ambient temperature and pressure.

Experimental methods	Author
Stagnation flame method	Wang et al. 2009 [6], Zhao et al. 2004 [7]
Spherical flame method	Wu et al. 2014 [8], Qin and Ju 2005 [9], de Vries et al. 2011 [10], Song et al. 2013 [11], Yu et al. 2014 [12], Huang et al. 2007 [13], Daly et al.2002 [14], Chen et al. 2009 [15], Chen et al. 2012 [16]
Heat flux method	Wang et al. 2018 [17]
Externally heated diverging channels method	Varghese et al. 2017 [18]
Annular stepwise diverging tubes method	Liu et al. 2013 [19], Liu et al. 2014 (9–11 L/min and 13-15 L/min) [20]

4.2. Influence of temperature

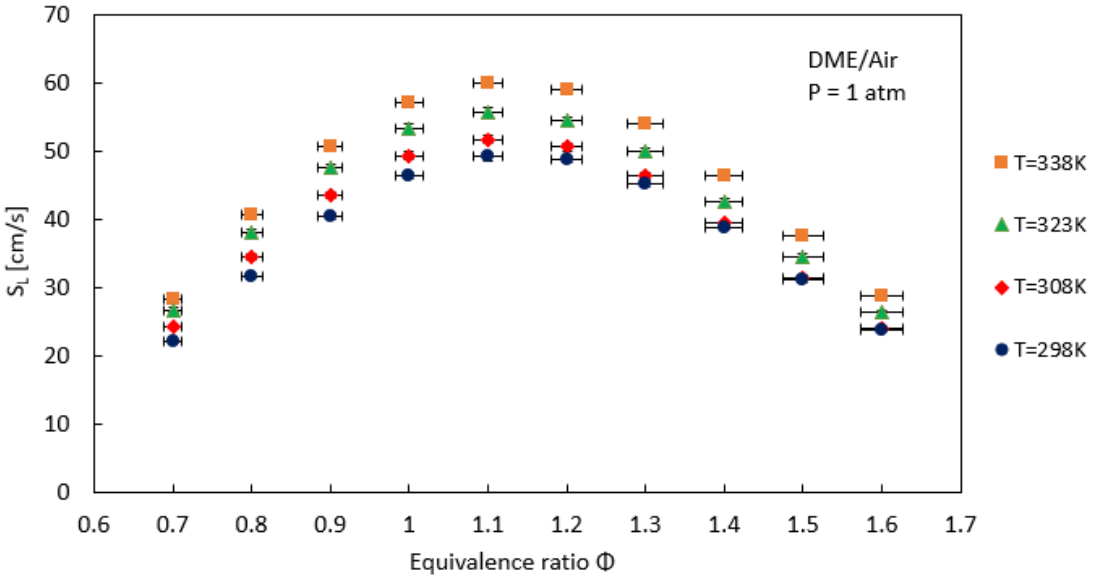

Figure 17: Experimental laminar burning velocity of DME/air mixtures at different initial mixed gas temperatures

The results of laminar burning velocity of DME at initial mixed gas temperatures of 298 K, 308K, 323 K and 338 K are presented in Figure 17. As expected, the laminar burning velocities increase with increasing initial mixed gas temperature. This is due to a higher initial temperature promotes the chemical reaction rates, causing an increase in the flame propagation rate. In addition, S_L (Φ) has similar trend at different temperatures. As the equivalence ratio increases, they all increase first and then decrease. This is resulted from the variation of the adiabatic flame temperature with equivalence ratio. When the equivalence ratio is relatively small, the combustion is complete, releasing same amount of heat as the stoichiometric conditions, but the adiabatic flame temperature is lower because there is excess oxygen and nitrogen that need to be heated up by the same amount of heat released. When the equivalence ratio is relatively large, the oxidizer in the mixtures is insufficient, and the combustion is incomplete. Compared with the heat release under fuel-lean and stoichiometric conditions, less heat is released, leading to lower adiabatic flame temperatures and lower chemical reaction rate. Moreover, for all studied temperatures, the highest S_L of experimental data is reached at $\Phi = 1.1$. This is because the adiabatic flame temperature is determined by the heat release of combustion and the heat capacity of the combustion products, which both decrease with the increase of equivalence ratio. Although complete combustion occurs at $\Phi = 1$ and generates the largest amount of heat, when Φ is slightly larger than 1, the reduction rate of the heat capacity of the combustion products is larger than the reduction rate of the heat release, causing a higher temperature of the combustion products.

(a)

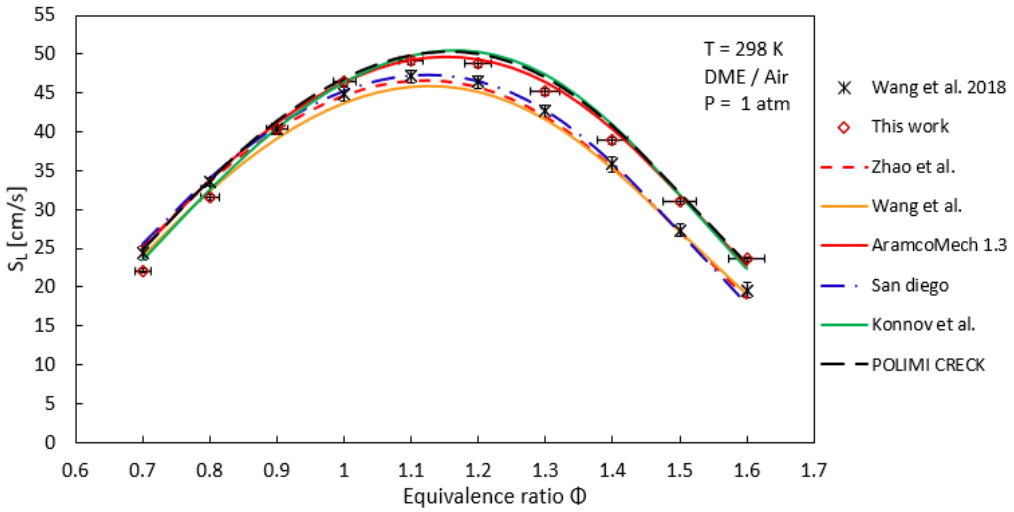
T = 298 K
DME / Air
P = 1 atm
Wang et al. 2018
This work
Zhao et al.
Wang et al.
AramcoMech 1.3
San diego
Konnov et al.
POLIMI CRECK
S_L [cm/s]
Equivalence ratio Φ

(b)

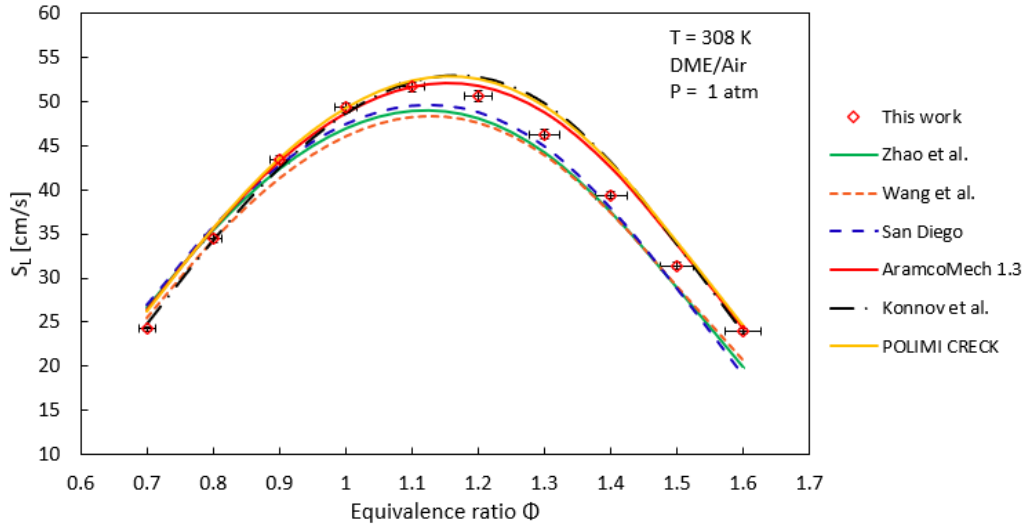
T = 308 K
DME/Air
P = 1 atm
This work
Zhao et al.
Wang et al.
San Diego
AramcoMech 1.3
Konnov et al.
POLIMI CRECK
S_L [cm/s]
Equivalence ratio Φ

(c)

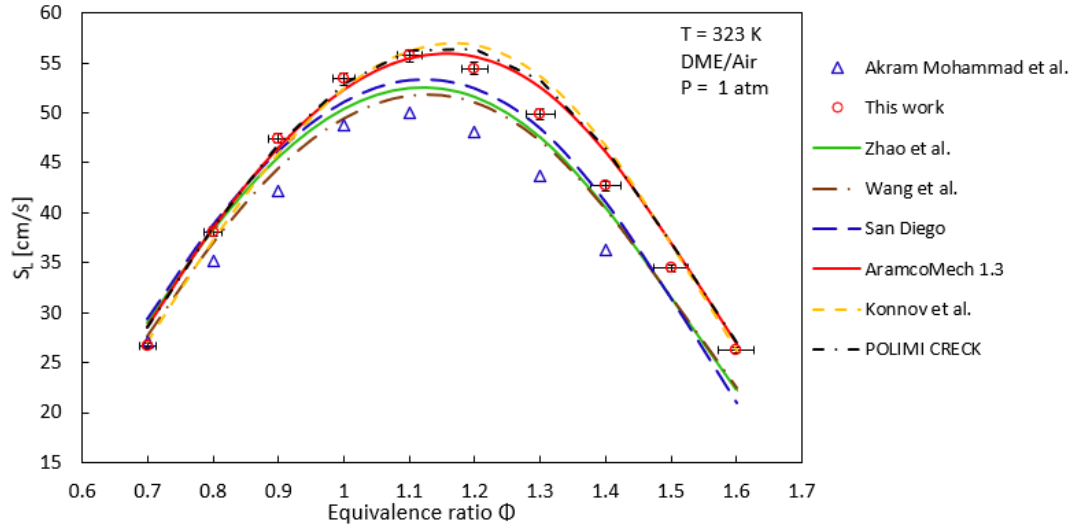
T = 323 K
DME/Air
P = 1 atm
Akram Mohammad et al.
This work
Zhao et al.
Wang et al.
San Diego
AramcoMech 1.3
Konnov et al.
POLIMI CRECK
S_L [cm/s]
Equivalence ratio Φ

（d）

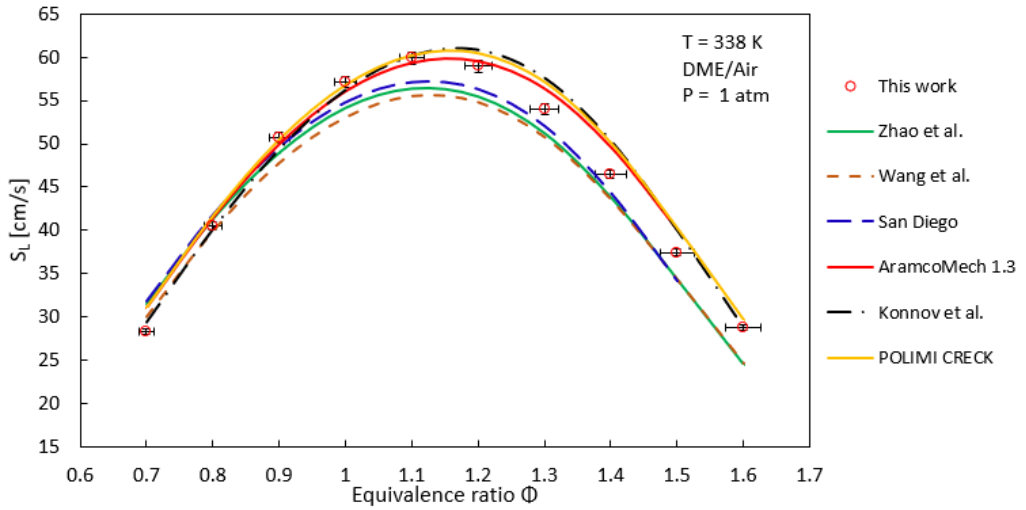

Figure 18: Laminar burning velocity of DME/air gas mixtures at different temperatures. (a) 298K, (b) 308 K, (c) 323 K, (d) 338 K.

The comparison of the present results with literature data and six mechanisms at T_g = 298 K-338 K and P = 1 atm are shown in Figure 18 (a), (b), (c), (d). The highest S_L of experimental data is reached at Φ = 1.1 at any inlet temperature, and this is also the largest S_L point of the simulation results of Zhao et al., Wang et al., and the San Diego models, while for Konnov et al., POLIMI CRECK and AramcoMech 1.3, the maximum S_L point appears at Φ = 1.2.

The consistency between experimental data and simulation results are similar at T_g = 298-338 K, see Figure 18 (a), (b), (c), (d). Zhao et al., Wang et al., and San Diego have similar S_L predictions; they overestimate S_L in fuel-lean conditions, while they underestimate it in fuel-rich conditions. Although Konnov et al., POLIMI CRECK, and AramcoMech 1.3 overestimate S_L in lean and rich conditions, they agree very well with experimental data under stoichiometric flames. Overall, AramcoMech 1.3 is the best mechanism in comparison to the data obtained from this work.

In addition to the six simulation results calculated from mechanisms available in literature and experimental results acquired at standard pressure and ambient temperature, Figure 18 (a) also includes data from Wang et al. 2018 [17], which were also measured using the heat flux method. However, data acquired in these two works are different, especially within Φ = 1.0-1.6, the deviation being 3-21%. Wang et al. 2018 data are slightly higher than the present data in fuel-lean conditions, while they are lower in fuel-rich conditions. The reason may be that the fuel purity is different, 99.9% in this work and 99.5 % in Wang et al. 2018, and the employed heat flux burners are also different.

Figure 18 (c) shows S_L data at T_g = 323 K acquired from this work and Mohammad et al. [52]. There is a significant disagreement between these two works, 8-17 %, except for Φ = 0.7, where the difference is only 1.5 %. The inconsistency of the data may be

due to the different experimental methods adopted. The externally heated diverging channels method was used by Mohammad et al. In this method, S_L is affected by heat loss, hydrodynamic stretching, and flame stability.

Overall, the results of this study agree well with the simulation results of POLIMI CRECK, Konnov et al., and AramcoMech 1.3 models at T_g = 298-338 K, especially when the equivalence ratio is in the range 0.8-1.1.

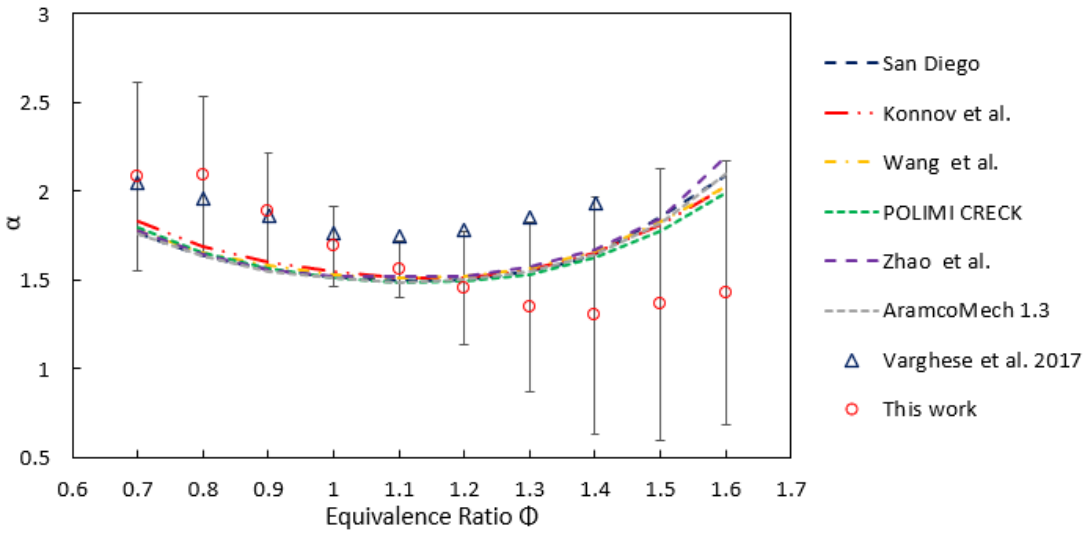

Figure 19: Relationship between the derived temperature dependence α and equivalent ratio Φ

Figure 19 illustrates the variation of the temperature dependence α of DME/air flames calculated from experimental data and kinetic mechanisms. According to the calculated results, the temperature exponent shows a non-linear relationship as a function of the equivalence ratio.

Data obtained by Varghese et al. using the externally heated diverging channels method in the temperature range from 350 to 640 K are also shown in Figure 19. It can be found that, in addition to the equivalence ratio, the temperature dependence of α is also affected by the measured temperature range and experimental method. Although the temperature exponent α derived from current work and literature data cannot completely overlap, they overlap within the uncertainty. Additionally, α values derived from the six simulation results are similar, and all of them agree with experimental results within the uncertainty of experimental data.

The uncertainty is very large at lean and rich conditions. Because of the small temperature range (40 K) in this measurement, the difference of S_L at different temperatures is also small at lean and rich conditions, leading to a non-linear relationship between $\frac{S_L}{S_{L,0}}$ and $\frac{T_u}{T_0}$. Therefore, in addition to the error caused by $\Delta S_L^{T_i}$ mentioned in Section 3.1.5, the error caused by fitting should also be considered. One approach to reduce the uncertainty is to increase the temperature range. However, in

order to stabilize the flame, the temperature difference ΔT between the unburned gas mixture and the burner plate must be at least 40℃. For example, in the measurements performed at T_g = 338 K, ΔT is only 30℃. Thus, when the flame reaches the adiabatic condition at Φ = 1.0-1.3, it is no longer flat, so S_L can only be obtained by extrapolation from sub-adiabatic condition.

4.3. NO mole fraction of DME / air gas mixtures at T_g = 338K

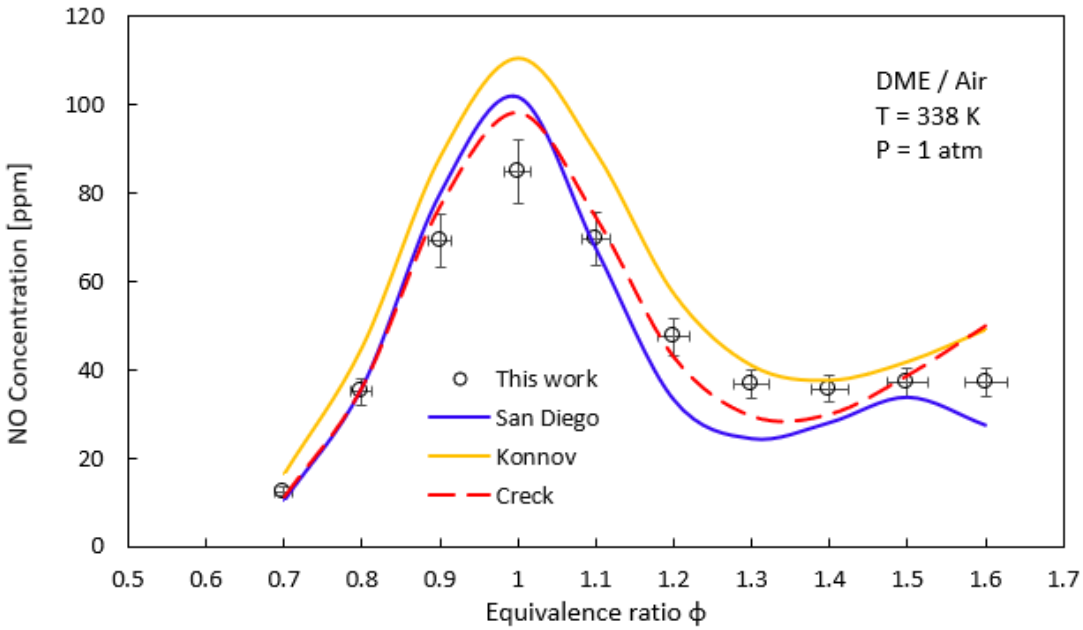

Figure 20: Experimental NO concentration of DME/air mixtures at T_g = 338 K.

Figure 20 shows simulation results and experimental data of NO mole fraction in DME flames at T_g = 338 K and P = 1 atm. The measuring point was located in the post-lame zone, 1 cm above the burner plate. The predicted trend of Konnov et al. and POLIMI CRECK mechanisms is similar to that of experimental data. NO concentration first reaches the maximum, about 85 ppm, at stoichiometric condition, and with the increase of equivalence ratio, the NO mole fraction decreases to about 36 ppm at $\Phi = 1.4$ and then remains rather constant with a value of 37 ppm at $\Phi = 1.5$ and 1.6. The NO concentration peak at stoichiometric flames is due to the fact that temperature reaches its maximum value here, and NO is generated through the thermal pathway [45]. The plateau observed in the NO mole fraction profile under fuel-rich conditions results from the prompt NO pathway, since a large amount of CH radicals is generated under rich conditions [45].

Although the predictions of the kinetic mechanisms show a similar trend compared to the experimental data, they do not completely overlap. All the mechanisms overestimate NO mole fractions around stoichiometric flames, about 16-30%. Although thermal NO formation near stoichiometric conditions is related to flame temperature, these experiments were performed at 1 cm above the burner plate, where the heat loss

is negligible. Hence, the disagreement between simulations and experimental results is due to the fact that thermal NO in the models is not well described.

Altogether, the POLIMI CRECK model shows the best agreement with the experimental data. The Konnov et al. model overestimates at both thermal NO and prompt NO. The thermal NO production using the San Diego model is also over-predicted around $\Phi = 1$, and prompt NO is under-predicted about 9-34%, but overall, it well predicts the experimental data. Therefore, in view of the discrepancies observed between the experimental data and the model predictions, this thesis provides additional high-fidelity benchmark data, which is essential for validation and further development of detailed kinetic models.

5. Conclusion

In this project, fundamental combustion properties of DME/air premixed flames were experimentally and numerically studied. One of the main goals of this thesis was to measure the laminar burning velocity of the DME/air flames at ambient and elevated temperature using the heat flux method, derive the temperature exponent, and validate the literature models using measured data. In addition, quantitative measurements of post-flame NO mole fractions obtained with the calibrated LIF technique to validate the existing models were also presented in detail in this thesis.

Laminar burning velocity of premixed DME/air mixtures

The laminar burning velocity of the DME/air mixtures was obtained in flat non-stretched flames at ambient and elevated temperatures. The results obtained were compared with experimental data available in the literature and with simulation results using existing models. Most literature data, simulation results and data acquired from this work have similar trends. As the equivalence ratio increases, S_L increases first and then decreases. For all studied temperatures, the highest S_L of experimental results are reached at $\Phi = 1.1$, and this is also the largest S_L point of the simulation results of Zhao et al., Wang et al., and the San Diego models, while for Konnov et al., POLIMI CRECK and AramcoMech 1.3, the maximum point appears at $\Phi = 1.2$. In addition, when the equivalence ratio $\Phi = 0.8$-1.0, Konnov et al., POLIMI CRECK, and AramcoMech 1.3 models match very well with experimental data in the present work, but they overestimate burning velocities under very fuel-rich conditions. For Zhao et al., Wang et al., and San Diego models, they under-predict burning velocities except for $\Phi = 0.7$ and 0.8. Overall, the AramcoMech 1.3 model shows the best consistency with the results presented in this work.

Although the experimental data obtained in this project deviate from the literature data measured in stretched flames, they can be regarded as high-value inputs for model validation. Additionally, the power exponent α, which expresses the dependence of laminar burning velocity on temperature, is also an important parameter for model validation. And since the practical combustion usually occurs under high temperature conditions that cannot be achieved by experiments, burning velocities used to design practical applications at these temperatures are derived from power exponent α.

Laser induced fluorescence of nitric oxide

NO concentration in the post flame zone of DME/air flames at 338 K were measured by the non-intrusive LIF technique. The experimental data acquired in this work are well predicted by literature mechanisms. As the equivalence ratio increases, the NO mole fractions first increase to a peak, about 85 ppm and then decrease to about 36 ppm,

and finally reach a plateau with a value of 37 ppm at very fuel-rich conditions. The first NO peak results from thermal NO formation, and the second increase is the formation of prompt NO. Under fuel-rich conditions, the experimental data agree very well with the Konnov et al. and POLIMI CRECK mechanisms, and the San Diego mechanism underestimates prompt NO formation. Overall, the experimental data are well predicted by POLIMI CRECK mechanism.

Altogether, the results obtained in present work can be considered as very valuable inputs for literature model validation and further development.

6. Outlook

This work was mainly focused on measuring the burning velocities and NO concentrations of premixed DME/air combustion at elevated temperatures to validate existing chemical kinetic models. The results show that there are discrepancies between the experimental results and the model predictions, and the literature models need to be improved.

Moreover, for the laminar burning velocity measurements, since the heating jacket around the burner plate of this heat flux burner is filled with water, the maximum temperature can only reach 368 K. In order to ensure that the flame that is stabilized on the burner plate under super-adiabatic conditions remains one-dimensional and flat, the maximum temperature of unburned gas mixtures can only be set to 338 K. In future research, other liquids with a higher boiling point can be used instead of water, such as oil, to obtain burning velocities in a wider temperature range to reduce the uncertainties in temperature dependence. In addition, the temperature dependence was derived by measuring S_L at different temperatures in present work. In further studies, the stagnation flame method and spherical method, which have a wider pressure range, can be employed to obtain S_L under different pressures to study the effect of pressure on S_L. Moreover, to gain more insight into the fundamental combustion properties of DME, measurements of DME/air mixtures blended with other fuels at various mixture fractions are also recommended.

Additionally, for the research on NO formation, the aim here was to measure accurate data to validate the existing mechanisms. In order to further understand the prediction difference of thermal NO and prompt NO among different mechanisms, sensitivity analyses can be performed on the simulation results related to NO formation under stoichiometric and fuel-rich conditions.

7. Acknowledgement

Finally, I am grateful to those who have provided me with encouragement and support during these nine months.

First and foremost, I would like to express my sincere gratitude to my supervisors *Alexander Konnov*, *Christian Brackmann* and *Marco Lubrano Lavadera* for their patient instruction and constructive advice. They have helped me a lot in choosing project topic, collecting materials, doing experiments and writing thesis. *Alexander*, I am grateful to your guidance and advice on the experiment. *Christian*, thank you for helping us optimize the experimental setups and giving me detailed answers when I had questions. *Marco,* I am deeply indebted to you for being with me throughout the whole experiment. And in the process of writing the thesis, your insightful comments on each draft provided me with many enlightening ideas and gave me helpful suggestions about academic writing. Moreover, I also want to thank *Per-Erik Bengtsson* and *Thi Kim Cuong Le* for helping me find this interesting project at Division of Combustion Physics. Everyone here is lovely and friendly. In addition, my thanks also go to examiners who will check this thesis. Your suggestions play an irreplaceable role in improving my academic knowledge. Finally, I would like to extend my deep gratefulness to my parents and friends for supporting me all the time and giving me help when I was trouble.

Reference

[1] Blaszczak, R., & Cox, L. (1999). Nitrogen oxides (NOx). Research Triangle Park, N.C.: U.S. Environmental Protection Agency, Office of Air Quality Planning and Standards, Information Transfer and Program Integration Division, Clean Air Technology Center.

[2] NO_x gases in diesel car fumes: Why are they so dangerous? (2020). Retrieved 19 April 2020, from https://phys.org/news/2015-09-nox-gases-diesel-car-fumes.html

[3] Konnov, A., Mohammad, A., Kishore, V., Kim, N., Prathap, C., & Kumar, S. (2018). A comprehensive review of measurements and data analysis of laminar burning velocities for various fuel+air mixtures. Progress In Energy And Combustion Science, 68, 197-267. doi: 10.1016/j.pecs.2018.05.003

[4] Hwang, C., Lee, C., & Lee, K. (2009). Fundamental Studies of NOx Emission Characteristics in Dimethyl Ether (DME)/Air Non-premixed Flames. Energy & Fuels, 23(2), 754-761. doi: 10.1021/ef800921q

[5] Jurchiş, B., Nicolae, B., Călin, I., & Nicolae Vlad, B. (2017). Study of emissions for a compression ignition engine fueled with a mix of DME and diesel. IOP Conference Series: Materials Science And Engineering, 252, 012065. doi: 10.1088/1757-899x/252/1/012065

[6] Wang, Y., Holley, A., Ji, C., Egolfopoulos, F., Tsotsis, T., & Curran, H. (2009). Propagation and extinction of premixed dimethyl-ether/air flames. Proceedings Of The Combustion Institute, 32(1), 1035-1042. doi: 10.1016/j.proci.2008.06.054

[7] Zhao, Z., Kazakov, A., & Dryer, F. (2004). Measurements of dimethyl ether/air mixture burning velocities by using particle image velocimetry. Combustion And Flame, 139(1-2), 52-60. doi: 10.1016/j.combustflame.2004.06.009

[8] Wu, H., Hu, E., Yu, H., Li, Q., Zhang, Z., Chen, Y., & Huang, Z. (2014). Experimental and Numerical Study on the Laminar Flame Speed of n-Butane/Dimethyl Ether–Air Mixtures. Energy & Fuels, 28(5), 3412-3419. doi: 10.1021/ef402502w

[9] Qin, X., & Ju, Y. (2005). Measurements of burning velocities of dimethyl ether and air premixed flames at elevated pressures. Proceedings Of The Combustion Institute, 30(1), 233-240. doi: 10.1016/j.proci.2004.08.251

[10] de Vries, J., Lowry, W., Serinyel, Z., Curran, H., & Petersen, E. (2011). Laminar flame speed measurements of dimethyl ether in air at pressures up to 10atm. Fuel, 90(1), 331-338. doi: 10.1016/j.fuel.2010.07.040

[11] Song, W., Jung, S., Park, J., Kwon, O., Kim, Y., & Kim, T. et al. (2013). Effects of syngas addition on flame propagation and stability in outwardly propagating spherical dimethyl ether-air premixed flames. International Journal Of Hydrogen Energy, 38(32), 14102-14114. doi: 10.1016/j.ijhydene.2013.08.037

[12] Yu, H., Hu, E., Cheng, Y., Zhang, X., & Huang, Z. (2014). Experimental and numerical study of laminar premixed dimethyl ether/methane–air flame. Fuel, 136, 37-45. doi: 10.1016/j.fuel.2014.07.032

[13] HUANG, Z., WANG, Q., YU, J., ZHANG, Y., ZENG, K., MIAO, H., & JIANG, D. (2007). Measurement of laminar burning velocity of dimethyl ether–air premixed mixtures. Fuel, 86(15), 2360-2366. doi: 10.1016/j.fuel.2007.01.021

[14] Daly, C. (2002). Burning velocities of dimethyl ether and air. Fuel And Energy Abstracts, 43(4), 275. doi: 10.1016/s0140-6701(02)86406-2

[15] Chen, Z., Wei, L., Huang, Z., Miao, H., Wang, X., & Jiang, D. (2009). Measurement of Laminar Burning Velocities of Dimethyl Ether−Air Premixed Mixtures with N_2 and CO_2 Dilution. Energy & Fuels, 23(2), 735-739. doi: 10.1021/ef8008663

[16] Chen, Z., Tang, C., Fu, J., Jiang, X., Li, Q., Wei, L., & Huang, Z. (2012). Experimental and numerical investigation on diluted DME flames: Thermal and chemical kinetic effects on laminar flame speeds. Fuel, 102, 567-573. doi: 10.1016/j.fuel.2012.06.003

[17] Wang, Z., Wang, S., Whiddon, R., Han, X., He, Y., & Cen, K. (2018). Effect of hydrogen addition on laminar burning velocity of CH_4/DME mixtures by heat flux method and kinetic modeling. Fuel, 232, 729-742. doi: 10.1016/j.fuel.2018.05.146

[18] Varghese, R., Kishore, V., Akram, M., Yoon, Y., & Kumar, S. (2017). Burning velocities of DME (dimethyl ether)-air premixed flames at elevated temperatures. Energy, 126, 34-41. doi: 10.1016/j.energy.2017.03.004

[19] Liu, Z., Lee, M., & Kim, N. (2013). Direct prediction of laminar burning velocity using an adapted annular stepwise diverging tube. *Proceedings Of The Combustion In*stitute, 34(1), 755-762. doi: 10.1016/j.proci.2012.06.080

[20] Liu, Z., & Kim, N. (2014). An assembled annular stepwise diverging tube for the measurement of laminar burning velocity and quenching distance. Combustion And Flame, 161(6), 1499-1506. doi: 10.1016/j.combustflame.2013.11.020

[21] Krejci, M., Mathieu, O., Vissotski, A., Ravi, S., Sikes, T., Petersen, E., Kérmonès, A., Metcalfe, W. and Curran, H. (2013). Laminar Flame Speed and Ignition Delay Time Data for the Kinetic Modeling of Hydrogen and Syngas Fuel Blends. Journal of Engineering for Gas Turbines and Power, 135(2), pp. 021503.

[22] Wang, Z., Zhang, X., Xing, L., Zhang, L., Herrmann, F., Moshammer, K., Qi, F. and Kohse-Höinghaus, K. (2015). Experimental and kinetic modeling study of the low- and intermediate-temperature oxidation of dimethyl ether. Combustion and Flame, 162(4), pp.1113-1125.1

[23] Zhao, Z., Chaos, M., Kazakov, A. and Dryer, F. (2008). Thermal decomposition reaction and a comprehensive kinetic model of dimethyl ether. International Journal of Chemical Kinetics, 40(1), pp.1-18.

[24] Prince, J., & Williams, F. (2015). A short reaction mechanism for the combustion of dimethyl-ether. Combustion and Flame, 162(10), 3589-3595. doi: 10.1016/j.combustflame.2015.06.016

[25] Capriolo, G., Brackmann, C., Lubrano Lavadera, M., Methling, T., & Konnov, A. (2020). An experimental and kinetic modelling study on nitric oxide formation in premixed C_3 alcohols flames. Submitted To Proceedings Of The Combustion Institute.

[26] Burke, U., Somers, K., O'Toole, P., Zinner, C., Marquet, N., & Bourque, G. et al. (2015). An ignition delay and kinetic modeling study of methane, dimethyl ether, and their mixtures at high pressures. Combustion And Flame, 162(2), 315-330. doi: 10.1016/j.combustflame.2014.08.014

[27] Frassoldati, A., Faravelli, T., Ranzi, E., Kohse-Höinghaus, K., & Westmoreland, P. (2011). Kinetic modeling study of ethanol and dimethyl ether addition to premixed low-pressure propene–oxygen–argon flames. Combustion And Flame, 158(7), 1264-1276. doi: 10.1016/j.combustflame.2010.12.015

[28] Song, Y., Marrodán, L., Vin, N., Herbinet, O., Assaf, E., & Fittschen, C. et al. (2019). The sensitizing effects of NO_2 and NO on methane low temperature oxidation in a jet stirred reactor. Proceedings Of The Combustion Institute, 37(1), 667-675. doi: 10.1016/j.proci.2018.06.115

[29] Metcalfe, W., Burke, S., Ahmed, S., & Curran, H. (2013). A Hierarchical and Comparative Kinetic Modeling Study of C_1− C_2 Hydrocarbon and Oxygenated Fuels. International Journal Of Chemical Kinetics, 45(10), 638-675. doi: 10.1002/kin.20802

[30] Bagheri, G., Ranzi, E., Pelucchi, M., Parente, A., Frassoldati, A., & Faravelli, T. (2020). Comprehensive kinetic study of combustion technologies for low environmental impact: MILD and OXY-fuel combustion of methane. Combustion And Flame, 212, 142-155. doi: 10.1016/j.combustflame.2019.10.0141

[31] Wu, C., & Law, C. (1985). On the determination of laminar flame speeds from stretched flames. Symposium (International) On Combustion, 20(1), 1941-1949. doi: 10.1016/s0082-0784(85)80693-7

[32] Dixon-Lewis, G. (1991). Structure of laminar flames. Symposium (International) On Combustion, 23(1), 305-324. doi: 10.1016/s0082-0784(06)80274-2

[33] Matalon, M. (2007). Intrinsic Flame Instabilities in Premixed and Nonpremixed Combustion. Annual Review Of Fluid Mechanics, 39(1), 163-191. doi: 10.1146/annurev.fluid.38.050304.092153

[34] Tien, J., & Matalon, M. (1991). On the burning velocity of stretched flames. Combustion And Flame, 84(3-4), 238-248. doi: 10.1016/0010-2180(91)90003-t

[35] VAN MAAREN, A., & DE GOEY, L. (1994). Stretch and The Adiabatic Burning Velocity of Methane- and Propane-Air Flames. Combustion Science And Technology, 102(1-6), 309-314. doi: 10.1080/00102209408935483

[36] Chao, B., Egolfopoulos, F., & Law, C. (1997). Structure and propagation of premixed flame in nozzle-generated counterflow. Combustion And Flame, 109(4), 620-638. doi: 10.1016/s0010-2180(97)89633-2

[37] Konnov, A., Dyakov, I., & De Ruyck, J . (2001). Probe sampling measurements and modeling of nitric oxide formation in methane + air flames. Combustion Science And Technology, 169(1), 127-153. doi: 10.1080/00102201089078431

[38] Knyazkov, D., Shmakov, A., Dyakov, I., Korobeinichev, O., De Ruyck, J., & Konnov, A. (2009). Formation and destruction of nitric oxide in methane flames doped with NO at atmospheric pressure. Proceedings Of The Combustion Institute, 32(1), 327-334. doi: 10.1016/j.proci.2008.06.037

[39] Konnov, A., Dyakov, I., Knyazkov, D., & Korobeinichev, O. (2010). Formation and Destruction of Nitric Oxide in NO Doped Premixed Flames of C_2H_4, C_2H_6, and C_3H_8 at Atmospheric Pressure. Energy & Fuels, 24(9), 4833-4840. doi: 10.1021/ef100527s

[40] Li, B., He, Y., Li, Z., & Konnov, A. (2013). Measurements of NO concentration in NH_3-doped CH_4+air flames using saturated laser-induced fluorescence and probe sampling. Combustion And Flame, 160(1), 40-46. doi: 10.1016/j.combustflame.2012.10.003

[41] Brackmann, C., Alekseev, V., Zhou, B., Nordström, E., Bengtsson, P., & Li, Z. et al. (2016). Structure of premixed ammonia + air flames at atmospheric pressure: Laser diagnostics and kinetic modeling. Combustion And Flame, 163, 370-381. doi: 10.1016/j.combustflame.2015.10.012

[42] Brackmann, C., Bood, J., Nauclér, J., Konnov, A., & Aldén, M. (2017). Quantitative picosecond laser-induced fluorescence measurements of nitric oxide in flames. Proceedings Of The Combustion Institute, 36(3), 4533-4540. doi: 10.1016/j.proci.2016.07.012

[43] Brackmann, C., Nauclér, J., El-Busaidy, S., Hosseinnia, A., Bengtsson, P., Konnov, A., & Nilsson, E. (2018). Experimental studies of nitromethane flames and evaluation of kinetic mechanisms. Combustion And Flame, 190, 327-336. doi: 10.1016/j.combustflame.2017.12.011

[44] Brackmann, C., Nilsson, E., Nauclér, J., Aldén, M., & Konnov, A. (2018). Formation of NO and NH in NH_3-doped $CH_4 + N_2 + O_2$ flame: Experiments and modelling. Combustion And Flame, 194, 278-284. doi: 10.1016/j.combustflame.2018.05.008

[45] Brackmann, C., Methling, T., Lubrano Lavadera, M., Capriolo, G., & Konnov, A. (2020). Experimental and modeling study of nitric oxide formation in premixed methanol + air flames. Combustion And Flame, 213, 322-330. doi: 10.1016/j.combustflame.2019.11.043

[46] Speight, J. (2011). Handbook of industrial hydrocarbon processes. Oxford: Gulf Professional.

[47] Alekseev, V. (2015). Laminar burning velocity of hydrogen and flame structure of related fuels for detailed kinetic model validation. Lund: Division of Combustion Physics, Department of Physics, Lund University.

[48] Bidabadi, M., Akbari Vakilabadi, M., Khoeini Poorfar, A., Monteiro, E., Rouboa, A. and Rahbari, A., 2016. Mathematical modeling of premixed counterflow combustion of organic dust cloud. *Renewable Energy*, 92, pp.376-384.

[49] Faghih, M., & Chen, Z. (2016). The constant-volume propagating spherical flame method for laminar flame speed measurement. Science Bulletin, 61(16), 1296-1310. doi: 10.1007/s11434-016-1143-6

[50] de GOEY, L., van MAAREN, A., & QUAX, R. (1993). Stabilization of Adiabatic Premixed Laminar Flames on a Flat Flame Burner. Combustion Science And Technology, 92(1-3), 201-207. doi: 10.1080/00102209308907668

[51] Akram, M., Kishore, V., & Kumar, S. (2012). Laminar Burning Velocity of Propane/CO_2/N_2–Air Mixtures at Elevated Temperatures. Energy & Fuels, 26(9), 5509-5518. doi: 10.1021/ef301000k

[52] Mohammad, A., & Juhany, K. (2019). Laminar burning velocity and flame structure of DME/methane + air mixtures at elevated temperatures. Fuel, 245, 105-114. doi: 10.1016/j.fuel.2019.02.085

[53] Laser-induced fluorescence spectroscopy: What's behind it? (2020). Retrieved 21 April 2020, from https://www.emg-automation.com/en/details/laserinduzierte-fluoreszenzspektroskopie-was-steckt-dahinter/

[54] Bosschaart, K. (2003). Detailed analysis of the heat flux method for measuring burning velocities. Combustion And Flame, 132(1-2), 170-180. doi: 10.1016/s0010-2180(02)00433-9

[55] Bosschaart, K. (2002). Analysis of the heat flux method for measuring burning velocities. Eindhoven: Technische Universiteit Eindhoven.

[56] Lavadera, M., & Konnov, A. (2020). Data Consistency of the Burning Velocity Measurements Using the Heat Flux Method: Syngas Flames. Energy & Fuels, 34(3), 3725-3742. doi: 10.1021/acs.energyfuels.9b03965

[57] Settersten, T., Patterson, B., & Gray, J. (2006). Temperature- and species-dependent quenching of NO A $^2\Sigma^+$ (v′=0) probed by two-photon laser-induced fluorescence using a picosecond laser. The Journal Of Chemical Physics, 124(23), 234308. doi: 10.1063/1.2206783

[58] Lubrano Lavadera, M.(2017). Combustion kinetic characteristics of smart energy carriers in model reactors (PhD thesis). Università degli Studi di Napoli Federico II.

[59] Han, X., Wang, Z., He, Y., Zhu, Y., & Cen, K. (2020). Experimental and kinetic modeling study of laminar burning velocities of NH_3/syngas/air premixed flames. Combustion And Flame, 213, 1-13. doi: 10.1016/j.combustflame.2019.11.032

[60] Marques, C., Barreta, L., Sbampato, M., & dos Santos, A. (2010). Laser-saturated fluorescence of nitric oxide and chemiluminescence measurements in premixed ethanol flames. *Experimental Thermal And Fluid Science*, *34*(8), 1142-1150. doi: 10.1016/j.expthermflusci.2010.04.003

Appendix

Table 1: Laminar burning velocities of DME/air mixtures at T_g = 298-338 K and P = 1 atm.

T_g (K)	Φ	ΔΦ	S_L (cm/s)	ΔS_L^+(cm/s)	ΔS_L^-(cm/s)
298	0.7	0.011879394	22.13822063	0.271768492	0.271967795
298	0.8	0.01357645	31.65652086	0.368587565	0.368707692
298	0.9	0.015273506	40.36623385	0.459150309	0.459211385
298	1.0	0.016970563	46.40338515	0.524682246	0.524722485
298	1.1	0.018667619	49.16636247	0.551781644	0.551776286
298	1.2	0.020364675	48.74569416	0.543313805	0.543325934
298	1.3	0.022061732	45.13983113	0.500802332	0.500878974
298	1.4	0.023758788	38.85240034	0.430133958	0.430272811
298	1.5	0.025455844	31.09735788	0.346252286	0.346567476
298	1.6	0.0271529	23.67007298	0.26696427	0.267342699
308	0.7	0.011879394	24.21129401	0.290387039	0.29054077
308	0.8	0.01357645	34.47168715	0.399613745	0.399662808
308	0.9	0.015273506	43.42027901	0.493712198	0.493745001
308	1.0	0.016970563	49.34482995	0.557559501	0.557567752
308	1.1	0.018667619	51.65748474	0.579519107	0.579518736
308	1.2	0.020364675	50.6017182	0.563756054	0.563766078
308	1.3	0.022061732	46.2917854	0.513143375	0.513176682
308	1.4	0.023758788	39.38246561	0.435627089	0.435755088
308	1.5	0.025455844	31.40963694	0.347823822	0.348055223
308	1.6	0.0271529	23.99472094	0.26929353	0.269695851
323	0.7	0.011879394	26.65741779	0.315335371	0.315443233
323	0.8	0.01357645	38.12959801	0.438734545	0.43880185
323	0.9	0.015273506	47.46745223	0.539789825	0.539849264
323	1.0	0.016970563	53.37899682	0.602512751	0.6024849
323	1.1	0.018667619	55.75849003	0.62524691	0.625179108
323	1.2	0.020364675	54.43032434	0.606836398	0.606869529
323	1.3	0.022061732	49.92197184	0.553744797	0.553823781
323	1.4	0.023758788	42.6701383	0.471607577	0.471748197
323	1.5	0.025455844	34.44282801	0.380562359	0.380766414
323	1.6	0.0271529	26.29559673	0.292989087	0.293342275
338	0.7	0.011879394	28.31090355	0.330309968	0.33040858
338	0.8	0.01357645	40.57167096	0.464965549	0.465025694
338	0.9	0.015273506	50.71419366	0.57658107	0.576604392
338	1.0	0.016970563	57.18638894	0.646421795	0.646551617

338	1.1	0.018667619	59.9126654	0.672148203	0.672263108
338	1.2	0.020364675	58.9647015	0.657882163	0.658029963
338	1.3	0.022061732	54.02021632	0.599240639	0.599370926
338	1.4	0.023758788	46.45859636	0.513321096	0.513509078
338	1.5	0.025455844	37.45077474	0.415348175	0.415582502
338	1.6	0.0271529	28.78254081	0.318428391	0.318719827

Table 2: NO mole fractions of DME/air mixtures at T_g = 338 K and P = 1atm.

T_g (K)	Φ	ΔΦ	X_{NO} (ppm)	ΔX_{NO} (ppm)
338	0.7	0.011879394	12.45786262	1.083834048
338	0.8	0.01357645	35.06262361	3.050448254
338	0.9	0.015273506	69.22337894	6.022433968
338	1.0	0.016970563	84.8609125	7.382899387
338	1.1	0.018667619	69.71805459	6.065470749
338	1.2	0.020364675	47.44911421	4.128072937
338	1.3	0.022061732	36.71060588	3.193822711
338	1.4	0.023758788	35.67560155	3.103777335
338	1.5	0.025455844	36.95464868	3.215054435
338	1.6	0.0271529	37.0305933	3.221661617